SLC4A1 MUTATIONS THAT CAUSE DISTAL RENAL TUBULAR ACIDOSIS ALTER CYTOPLASMIC PH AND CELLULAR AUTOPHAGY

Grace Essuman[1], Midhat Rizvi[1], Ensaf Almomani[6], Shahid A. K M. Ullah[1,5], Sarder M. A. Hasib[3], Forough Chelangarimiyandoab[1], Priyanka Mungara[1], Manfred J. Schmitt[3], Marguerite Hureaux[2], Rosa Vargas-Poussou[2], Nicolas Touret[4] & Emmanuelle Cordat[1*]

[1]Department of Physiology, University of Alberta, Edmonton, AB, Canada.
[2]Department of Genetics, Georges Pompidou European Hospital, Paris, France.
[3]Department of Molecular and Cell Biology, Department of Biosciences (FR 8.3) and Center of Human and Molecular Biology (ZHMB), Saarland University, Saarbrücken, Germany.
[4]Department of Biochemistry, University of Alberta, Edmonton, AB, Canada.
[5]Department of Medicine, University of Alberta, Edmonton, AB, Canada.
[6]Department of Basic Medical Sciences, Faculty of Medicine, Al-Balqa Applied University, Al-Salt, Jordan

[*] To whom correspondence should be addressed: Department of Physiology, Membrane Protein Disease Research Group, Room 7-34, Medical Sciences Building, University of Alberta, Edmonton, Alberta, T6G 2H7, Canada, Tel: 780-492-0209, Fax: 780-492-8915, e-mail: cordat@ualberta.ca

Key words: kidney, transporters, membrane protein, acidosis, epithelium, trafficking, distal renal tubular acidosis, autophagy, lysosome.

Abstract

Distal renal tubular acidosis (dRTA) is a disorder characterized by the inability of the collecting duct system to secrete acids during metabolic acidosis. The pathophysiology of dominant or recessive *SLC4A1* variant related dRTA has been linked with the mis trafficking defect of mutant kAE1 protein. However, *in vivo* studies in kAE1 R607H dRTA mice and humans have revealed a complex pathophysiology implicating a loss of kAE1-expressing intercalated cells and intracellular relocation of the H^+-ATPase in the remaining type-A intercalated cells. These cells also displayed accumulation of ubiquitin and p62 autophagy markers. The highly active transport properties of collecting duct cells require the maintenance of cellular energy and homeostasis, a process dependent on intracellular pH. Therefore, we hypothesized that the expression of dRTA variants affect intracellular pH and autophagy pathways. In this study, we report the characterization of newly identified dRTA variants and provide evidence of abnormal autophagy and degradative pathways in mouse inner medullary collecting duct cells and kidneys from mice expressing kAE1 R607H dRTA mutant protein. We show that reduced transport activity of the kAE1 variants correlated with increased cytosolic pH, reduced ATP synthesis, attenuated downstream autophagic pathways pertaining to the fusion of autophagosomes and lysosomes and/or lysosomal degradative activity. Our study elucidated a close relationship between the expression of defective kAE1 proteins, reduced mitochondrial activity and decreased autophagy and protein degradative flux.

Introduction

Distal renal tubular acidosis (dRTA) is a disorder characterized by the inability of the collecting duct system to secrete acids during metabolic acidosis[1]. In addition to hyperchloremic metabolic acidosis, patients with this disease can present with hypokalemia, kidney stones, urinary sodium waste and difficulty to thrive. Expression of pathogenic variants in the *ATP6V0A4*, *ATP6V1B1*, *FOXI1*, *WDR72* and *SLC4A1* genes are the usual genetic aetiologies[2–4]. The *SLC4A1* gene encodes the anion exchanger 1 (AE1) protein, which is an electroneutral chloride/bicarbonate exchanger[5]. It exists in two forms: a 911 amino acid erythroid isoform known to interact with erythroid cytoskeletal proteins and participate in red cell respiration and integrity, and a 65 amino acid (NH_2-terminal) truncated isoform primarily found in the basolateral membrane of renal type A intercalated cells (A-IC)[6,7] and podocytes[8]. This isoform participates in bicarbonate reabsorption and through its physical and functional interaction with the cytosolic carbonic anhydrase II and apical H^+-ATPase, it supports apical proton export and urine acidification[9].

Pathogenic variants in the *SLC4A1* gene can result in either red cell defects (such as Southeast Asian ovalocytosis[10,11] and hereditary spherocytosis[12]), renal cell defects (dRTA[10]) or both in patients with homozygous (Band 3 Coimbra and Band 3 Courcouronnes[13,14]) or compound heterozygous variants[15,16]. Renal *SLC4A1* disease-causing variants have only been found in the transmembrane domain - where it could impact protein structure and its transport function- or in the short carboxyl domain – where it possibly affects protein-protein interactions. The pathophysiology of dominant or recessive *SLC4A1* related dRTA (hereafter named dRTA) has originally been linked with the mis-trafficking defect of mutant kAE1 protein[10,17]. However, recent *in vivo* studies in R607H (orthologous to human R589H dRTA variant) and L919X knockin mice and dRTA patients have revealed a complex

pathophysiology where kAE1-expressing intercalated cells were lost, and in the remaining type-A intercalated cells, the H^+-ATPase relocated intracellularly and accumulated autophagy marker p62 and ubiquitin-positive material[18].

The highly active transport properties of collecting duct cells require the tight maintenance of cellular energy and homeostasis. The autophagy-mediated turnover of damaged organelles is necessary for protecting collecting duct cells as in most renal cells[19]. The chloride/bicarbonate exchange function of kAE1 in A-ICs confers a pivotal role in pH homeostasis and thus is a major contributor to cellular homeostasis. kAE1 protein interacts with several proteins such as integrin-like kinase (ILK), adaptor-related protein complex 1, 3 & 4 (AP-1, AP-3 & AP-4 mu1A), transmembrane protein 139 (TMEM139), kinesin family member 3B (KIF3B), and clathrin among others[7,20–22] that support protein stability and trafficking. It also interacts with homeostatic proteins including the glycolytic enzyme glyceraldehyde-3-phosphate dehydrogenase (GAPDH)[23] and the antioxidant enzyme peroxiredoxin 6 (PRDX 6)[24], which play major roles in cellular energy metabolism and oxidative stress response, respectively.

In this study, we report the characterization of newly identified dRTA genetic variations and provide evidence of abnormal autophagy and degradative pathways in cells and kidneys from mice expressing dRTA mutant kAE1 proteins.

Concise Methods

Ethics Approval

This study was conducted in accordance with all national and institutional animal care guidelines and approved by the University of Alberta's Animal Care and Use Committee (AUP #1277).

Newly identified *SLC4A1* variations from dRTA patients

The patient carrying the R295H mutation was a boy carrying the variation in the homozygous state, whose genetic diagnosis was made at the age of 5, following growth retardation of -2 SD for both weight and height, with bicarbonate at 18 mmol/L, potassium at 2.8 mmol/L, chloridemia at 94 mmol/L, calcemia at 2.55 mmol/L, and a urinary pH of 7.5. He also had a history of a pyeloureteral junction syndrome that was surgically managed at the age of 3. The R295H dRTA variation is a nonsense homozygous substitution characterized by a replacement of guanine (G) on position 884 by adenine (A) in the coding sequence. It has an allelic frequency of 0.14 % in the European population.

For the Y413H variant, the patient was a female diagnosed at 1 month old, with an urinary pH of 7.5, evidence of nephrocalcinosis and failure to thrive. The S525F variant has been previously reported[25], but in brief, the patient was a 13 year old female with plasma pH of 7.25, plasma bicarbonate at 15.3 mmol/L who also presented with polyurethral junction syndrome, nephrocalcinosis and nephrolithiasis since childhood. The Y413H and S525F dRTA variations are nonsense heterozygous substitutions characterized by a replacement of thymine (T) at position 1237 by cytosine (C) and a replacement of cytosine (C) at position 1574 by thymine (T), respectively. The R589H dRTA variation has been previously described[18]. No follow up data were available for all patients.

116

117 **Mice**

118 Transgenic mice carrying the R607H knockin (KI) mutation (murine equivalent to human
119 R589H mutation) were previously described[18]. Homozygous mice used throughout the study
120 display incomplete dRTA with alkaline urine without metabolic acidosis at baseline as
121 previously reported[18]. Homozygous mice or wild-type (WT) littermates were fed a standard
122 rodent chow (Picolab® Rodent Diet 20 # 5053, LabDiet, ST. Louis, MO, USA) or for Figure
123 5 (H-K), a salt-depleted diet with acid challenge as previously reported[26] with adequate and
124 constant water supply, and maintained on a 12-hour light and dark cycle throughout their
125 lifespan.

126

127 **Statistical analysis**

128 All the experiments were independently repeated a minimum of three times. Experimental
129 results were analyzed using the GraphPad Prism software and are summarized as mean ±
130 SEM. All statistical comparisons were made using unpaired Student's t test or one/two-way
131 ANOVA followed by a post-hoc test as indicated in figure legends. A P-value less than 0.05
132 was considered statistically significant. All datasets were assessed for normality, and outliers
133 identified by Prism were excluded.

134

135 Detailed Material and Methods are listed in the Supplementary Material.

136

Results

The dRTA kAE1 variants traffic to the basolateral membrane but have reduced transport activity in mIMCD3 cells.

We first characterized three newly identified dRTA mutations and compared them with kAE1 WT or previously characterized kAE1 R589H mutant. **Figure 1A** depicts the alpha fold predicted structure of kAE1 showing amino acids mutated in each kAE1 mutant. kAE1 R295H is a recessively inherited substitution in the N-terminal cytosolic domain of the protein. kAE1 Y413H is a dominantly inherited substitution in transmembrane domain (TM) 1 of the core domain. In the gate domain, dominantly inherited S525F and R589H substitutions occur in TM 5 and TM 6, respectively. We generated the newly identified dRTA variant cDNAs and expressed them or kAE1 WT in mIMCD3 cells. As seen on **Figure 1B,** kAE1 R295H, S525F and R589H variants display 2 typical bands similar to kAE1 WT. The top band (open circle) encompasses kAE1 proteins carrying a complex oligosaccharide that have reached the Golgi and beyond, while the bottom band (black circle) corresponds to high mannose-carrying kAE1 proteins located in the endoplasmic reticulum. However, kAE1 Y413H mutant bands intensity was overall weaker than WT and displayed a predominant single band aligned with high mannose-carrying kAE1 proteins. These results indicate that the 3 newly described dRTA mutants are successfully expressed in mIMCD3 cells. We next localized these mutants by immunofluorescence in polarized mIMCD3 cells. Both kAE1 WT and mutants appropriately co-localized with basolateral membrane marker beta-catenin in polarized mIMCD3 cells **(Figure 1C)**. kAE1 R589H location has previously been reported at the basolateral membrane in polarized mIMCD3 cells[18]. However, staining for kAE1 Y413H was again weaker and seemed more intracellular than other mutants. To address a possible premature degradation of this variant, we measured its lifetime and observed that its

degradation begins 6 hours post-synthesis while kAE1 WT abundance remained stable for 24 hours (**Figure 1D**). Finally, to assess the transport activity of the mutants, we examined the steady-state cytosolic pH (pHi) and rate of intracellular alkalinisation of mIMCD3 cells expressing kAE1 WT or mutants (**Figure 1E-G**). Using BCECF-AM, we observed that the steady state intracellular pH (pHi) of kAE1 mutant cells was more alkaline than WT cells (except for kAE1 R295H cell pHi, which has a similar trend but is not significantly different from WT) (**Figure 1F**), in agreement with rate of intracellular alkalinisation (**Figure 1G**). Note that transport activity, measured as rate of alkalinisation, is measured by reverting kAE1 exchange activity from bicarbonate *export* to *import* (see Methods, protocol for transport assay), hence a reduced alkalinisation rate is observed in cells expressing defective kAE1 protein compared to WT (**panel G**). Overall, these results indicate that except for kAE1 Y413H mutant, the other newly described variants are expressed and traffic to the basolateral membrane of polarized mIMCD3 cells, similar to the previously published kAE1 R589H mutant. Given that the premature degradation of kAE1 Y413H mutant likely explains the dRTA phenotype, we did not perform further assays on cells expressing this protein.

Autophagy processes are altered in mIMC3 cells expressing the kAE1 R295H, S525F and R589H dRTA mutants and in R607H knockin kidney lysates.

In mice expressing kAE1 R607H (the murine equivalent to human dRTA R589H substitution), a striking reduction in type-A intercalated cells was noted and in the remaining cells, autophagy marker p62 and ubiquitin accumulated in these abnormally enlarged cells[18]. We therefore investigated the autophagy machinery in dRTA mutant mIMCD3 cells and in R607H knockin (KI) mice. We first examined the ratio of autophagosome marker LC3BII protein relative to the total intensities of LC3BI and LC3BII as well as p62 levels. These experiments were performed at steady state, upon autophagy induction by starvation, or after

autophagy inhibition by Bafilomycin (Baf) A1 **(Figure 2A-C)**. **Figure 2A – I** shows a consistent increase in the ratio of LC3B II to total LC3B (I + II) in the mutant cells at steady state (**panel D**), with starvation (**panel F**) and with Baf A1 (**panel H**) except for the kAE1 R295H mutant which was not significantly different from WT. This suggests an altered autophagy process in the mutant cells, in agreement with preliminary findings from Mumtaz and colleagues[18]. There was no significant difference in p62 abundance in mutant cells compared to WT at steady state and with starvation (**Figure 2E&G**). However, with Baf A1, R589H mutant cells had significantly lower p62 abundance compared to WT (**Figure 2I**). To confirm these findings, we next assessed the abundance of these markers in whole kidney lysates from the kAE1 R607H KI mice. We observed that the total LC3B abundance was significantly higher in homozygous KI mice (KI/KI) compared to WT, with no difference in p62 (**Figure 2J-L)**. Overall, these results suggest an abnormal autophagy in mutant mIMCD3 cells and in kidneys of R607H KI mice. Given the lack of difference in phenotype between the recessive kAE1 R295H and kAE1 WT mIMCD3 cells, we focused the subsequent experiments on dominant kAE1 S525F and R589H mutant cells. Further investigations will be needed to understand the pathophysiology associated with the kAE1 R295H novel variant.

Late autophagy steps are blocked in dRTA kAE1 mutant-expressing cells due to their alkaline intracellular pH.

Given these preliminary findings of abnormal autophagy in dRTA mutant cells, we examined in more detail their autophagy machinery by transiently transfecting them with the eGFP-RFP-LC3 construct and monitoring the rate of autophagosome and autolysosome formation. In this assay, the green fluorescent protein (eGFP) fused to LC3 is quenched in the acidic environment of the autolysosome, while both eGFP and red fluorescent protein (RFP) fluoresce in vesicles in the neutral lumen of the autophagosome[27,28]. To avoid the poor

efficiency of transient transfection in polarized cells, experiments were conducted in sub-confluent cells pending that the mutant proteins are present at the plasma membrane. We therefore performed cell surface biotinylations on 70-80 % sub-confluent cells, which confirmed a robust plasma membrane abundance of both kAE1 R589H and S525F that was not significantly different from the WT protein (**Figure 3A&B**). Therefore, we next assessed the efficiency of the autophagy machinery in WT or dRTA mutant-expressing cells (**Figure 3C-F**). Focusing on cells expressing either kAE1 WT, kAE1 S525F or R589H, we quantified the number RFP+ (red, acidic autolysosomes) and double eGFP+/RFP+ (yellow, not acidic autophagosomes) vesicles. kAE1 S525F mutant cells have significantly more autophagosomes than WT counterparts (**Figure 3D),** and both kAE1 S525F and R589H have significantly more autolysosomes than WT (**Figure 3E). Figure 3F** shows that both mutants had significantly more autophagosomes (yellow) than autolysosomes (red). This finding suggests an upregulation of autophagy and inhibition in the downstream steps of the process that involves the fusion of autophagosomes with the lysosome[29]. As autolysosomes require luminal v-H^+-ATPase-dependent acidification to efficiently clear cell debris [30], the higher intracellular pH seen in mutant cells (**Figure 1F**) may be detrimental to v-H^+-ATPase full activity and impair proper autolysosomal acidification[31]. We therefore wondered whether chemically acidifying the pHi in mutant cells would rescue the autophagy machinery (**Figure 3G-K)**. We first determined that incubation of mIMCD3 cells in 0.033 μM nigericin in cell culture medium at pH 6.6 for 2 hours acidified cytosolic pH to 6.9 without causing cell death (**Supplementary Figure 1A-C**). Next, we observed that chemically reducing pHi to 6.9 in mutant expressing cells reduced the ratio of LC3B II to total LC3B (**Figure 3J)** and the abundance of lysosomal-associated membrane protein 1 (LAMP1) in R589H cells (**Figure 3 K)** to levels similar to WT cells at steady state. These findings suggest that abnormal

autophagy in the mutant cells may be caused by their alkaline pHi, resulting from a reduced anion exchange activity of the mutant kAE1 protein.

mIMCD3 cells expressing dRTA kAE1 mutants and R607H KI kidney tissues have abnormal lysosome number and size.

The accumulation of autophagosomes and autolysosomes as seen above may suggest one or a combination of the following: an inability of autophagosomes to fuse with lysosomes and/ or a defect in lysosomal degradative activity in the mutant cells[19,32]. We first examined the lysosomal degradative activity by assessing lysosomal protease Cathepsin B activity using Magic Red staining, a probe that fluoresces upon lysosomal protease cleavage (**Figure 4A-B).** In agreement with increased RFP+ vesicles (**Figure 3E**), the kAE1 S525F mutant cells had a significantly higher number of Magic Red positive vesicles than WT whereas the kAE1 R589H mutant cells had significantly larger Magic Red positive vesicles, suggesting an accumulation of undigested material[33]. To validate this finding *in vivo*, we performed immunostaining and quantified LAMP1 positive staining in ß1 ATPase positive cells (a marker of ICs) in WT and R607H KI mouse kidney sections. The KI mice showed significantly more and larger LAMP1 positive vesicles compared to WT mice in both cortex and medulla (**Figure 4 C-F**). We probed further into the lysosomal activity by quantifying lysosomal protease Cathepsin D (immature, intermediate and mature) protein abundance by immunoblot in isolated primary murine A-ICs. Although the abundance of immature and intermediate cathepsin D did not differ between genotypes, the KI mice showed a significantly decreased abundance of mature cathepsin D (**Supplementary Figure 2**). Thus, in line with *in vitro* findings, A-IC from homozygous R607H KI mice display relatively more and larger lysosomes with reduced active protease abundance than WT littermates, suggesting a lysosomal defect in the dRTA kAE1 mutant cells.

dRTA kAE1 mutant cells have lower ATP production rate and abnormal mitochondrial content.

Lysosomal degradation is highly dependent on a low luminal pH generated in part by the vacuolar-type H^+-ATPase[34] whose activity depends on ATP hydrolysis. We therefore analysed the ATP production rate in mIMCD3 cells, specifically glycolysis and oxidative phosphorylation. We measured the oxygen consumption rate (OCR) (**Figure 5A**) and extracellular acidification rate (ECAR) (**Figure 5B**) in empty vector transfected, kAE1 WT or mutant cells. Both kAE1 S525F and R589H mutant cells had a lower ATP production rate compared to WT (**Figure 5C**). More specifically, the R589H mutant cells had a lower mitochondrial ATP production rate (**Figure 5D**) whereas the kAE1 S525F mutant cells exhibited a lower glycolytic ATP production rate (**Figure 5E**). With the mitochondria being the major ATP-producing organelles[35], we assessed mitochondrial content by immunostaining of translocase of the outer membrane 20 (TOM20) both *in vitro* and *in vivo.* Both kAE1 S525F and R589H mutant cells have higher mitochondrial content compared to WT as determined by total overall intensity of TOM20 positive puncta (**Figure 5F&G**). In line with this result, although a decreased fluorescence intensity was observed in the cortex, there was a significantly higher TOM20 fluorescence intensity in medullary kidneys of homozygous R607H KI mutant mice compared to WT littermates (**Figure 5H-K**).

Discussion

In this study, we characterized three newly identified dRTA-causing kAE1 variations. Combining *in vivo* and *in vitro* studies, we demonstrated that reduced transport activity of the kAE1 mutants correlated with increased cytosolic pH, reduced ATP synthesis, attenuated downstream autophagic pathways and lysosomal dysfunction, pertaining to the fusion of autophagosomes and lysosomes and/ or lysosomal degradative activity (See summary in **Supplementary Tables 1 & 2**).

In line with previous observations in mIMCD3 cells[18], the kAE1 R295H, Y413H and S525F mutants were properly localized to the basolateral membrane after polarization. When expressed in Madin-Darby canine kidney (MDCK) cells, other dRTA-causing kAE1 mutants such as dRTA R602H, G701D, V488M, deltaV850 variants exhibited a plasma membrane trafficking defect[10,36,37]. In contrast, the kAE1 R589H mutant was correctly targeted to the plasma membrane[18]. Functionally, cells expressing the Y413H and S525F mutants exhibit about 60 % reduction in chloride/bicarbonate exchange activity compared to kAE1 WT, similar to the previously characterized recessive G701D mutant but unlike the R295H mutant[38]. Therefore, the mechanism causing dRTA remains unclear in the case of the newly identified recessive R295H variant. Additionally, the kAE1 Y413H variant exhibited a shorter half-life than WT counterpart, likely explaining dRTA, and thus was not further investigated. These findings add to the growing list of *SLC4A1* gene variations causing dRTA.

We next investigated the roots of the altered autophagy briefly reported in R607H KI mice[18] using mIMCD3 cells and whole kidney lysates. In kidneys of the KI mice, a decrease in the number of A-IC, accumulation of p62 and ubiquitinylated proteins and enlarged remaining A-ICs, suggested altered autophagy processes in dRTA mutant cells and in homozygous R607H KI mice[18,38]. During the autophagy process, LC3B I (a marker for

autophagosomes) is converted to lipidated LC3B II[39] and p62 aggregates to facilitate the degradation of ubiquitinated proteins within the autophagosome complex[40]. In mIMCD3 cells expressing dRTA kAE1 S525F and R589H variants, LC3B lipidation was increased compared to WT, an increase that persisted with both Baf A1 treatment and starvation. Although opposite effects were expected under inhibition or induction of autophagy, such similar effect has been previously described. In the proximal tubule of obese mice, LC3B accumulation indicating a stagnated autophagy flux, was observed with both chloroquine treatment and 24 hour starvation[41]. Similarly, in NRK-52E cells, a disruption of the autophagy machinery in high cadmium-stressed cells resulted in LC3B II accumulation under either Baf A1 or rapamycin (an autophagy inducer) treatment[42]. Although LC3B II is elevated during both increased autophagy flux and disrupted autophagy, we did not observe significant accumulation of p62 in mIMCD3 cells expressing dRTA mutants. p62 is specifically a marker of autophagy-mediated protein clearance[43–45]. Therefore, p62 accumulation in R607H KI mouse kidney sections strongly suggests a compromised autophagy-mediated clearance while the increased LC3B lipidation without significant changes in p62 in mIMCD3 cells points towards either an increased autophagic flux and/or a disrupted autophagy.

To obtain a clearer picture of the precise autophagic pathway altered in the dRTA mutants, we probed further into the different stages of autophagy and autophagy flux. We noted an accumulation of autophagosomes and autolysosomes in the S525F and R589H mutant cells. This was recapitulated in the R607H KI mice which showed significantly more and larger LAMP 1 positive vesicles in both kidney cortex and medulla, suggesting a blockage in late steps of autophagy flux in both dRTA mutant cells and KI mice. Such blockage has been implicated in the pathophysiology of several diseases. In lysosomal storage disease, lysosome accumulation in proximal tubule cells is a key component in the pathways mediating epithelial dysfunction[19]. In this study, restoring autophagy flux

attenuated disease progression. Another study in SK-N-SH, RT4-D6P2T and HeLa cells implicated autophagosome and lysosome accumulation in cellular toxicity associated with neurodegenerative diseases[32]. In agreement with altered lysosomal function, we also noted a greater abundance and size of active cathepsin B lysosomal protease vesicles in mIMCD3 cells. Increased cathepsin B activity affects lysosomal biogenesis, autophagy initiation and cellular homeostasis[46]. In the renal context, cathepsin B knockout mice demonstrated a higher resistance and quicker recovery from glomerular damage[47], suggesting that cathepsin B accumulation may be detrimental to the cells. Increased cathepsin B abundance in the dRTA mutant cells also correlates with the accumulation of lysosomes. Overall, these findings suggest that the pathogenesis of dRTA in our *in vitro* and *in vivo* models involves an inhibition of autophagy flux at the downstream steps involving autophagosome-lysosome fusion and lysosomal protein clearance [29,33,48,49].

The question remained as to how these dRTA variants altered autophagy. The *SLC4A1-3* gene family that includes AE1 are regulators of intracellular pH in different cell types[50–52]. The reduced anion exchange activity in mIMCD3 cells expressing the R589H and S525F variants expectedly correlated with an increased pHi compared to WT counterparts. Given that pHi variations can impact autophagy[31,34,53–55], we wondered whether this was the case for cells expressing kAE1 dRTA mutants. We observed that an acidic pHi in mutant cells restored autophagy levels similar to WT. Previous studies reported more perinuclear localization of lysosomes and autophagosome-lysosome fusion in cells with an increased pHi[53,54]. Although not examined in our study, an increase in intracellular pH due to starvation decreased the levels of lysosomal kinesin superfamily member KIF2 and ADP-ribosylation factor-like 8B (ARL8), which are responsible for redistributing lysosomes to the cell periphery. This reduction subsequently inhibited mTORC1, resulting in increased autophagosome synthesis and autophagosome-lysosome fusion[53].

While an alkaline cytosolic pH partially explains the impairment in autophagy flux, a close relationship also exists between intracellular pH and cellular energy dynamics and metabolic stress, all of which are key regulators of autophagy[56]. Therefore, it was plausible that kAE1 variant-induced autophagy dysregulation occurs through a signalling pathway akin to that of energy deprivation-induced autophagy. This hypothesis is supported by our findings of reduced ATP production rate in dRTA kAE1 S525F and R589H mutant cells compared to kAE1 WT cells. We also found that both kAE1 S525F and R589H mutant cells have higher mitochondrial content compared to kAE1 WT cells. The increased mitochondrial content coupled with low ATP point towards improper mitochondrial function in dRTA variant cells. Low ATP levels as seen in dRTA mutant cells may impair autophagy as was shown in human RPE cells[57]. ATP reduction in RPE cells led to complex mitochondrial changes such as structural disorganization, enzyme activity decline, and oxidative damage to mitochondrial components and DNA[57]. Similarly, in pancreatic islet cells, an alkaline pHi led to increased uptake of phosphate by mitochondria, accelerating the production of superoxide, promoting mitochondrial permeability transition, and inducing translational attenuation due to endoplasmic reticulum stress, ultimately impairing insulin secretion[58]. Overall, our data support that expression of the kAE1 variants increases pHi which alters mitochondrial function and leads to reduced cellular energy levels that eventually attenuates energy-dependent autophagic pathways including autophagosome-lysosome fusion and lysosomal protein clearance.

In light of these observations, we postulated that correcting the alkaline pHi of dRTA mutant-expressing mIMCD3 cells will alleviate this blockage in autophagy flux. We observed that a chemically engineered pHi of 6.9[59] reduced LC3B II accumulation and LAMP1 abundance in mIMCD3 mutant cells to expression levels similar to that of WT cells at baseline. This suggests that a chemically reduced pHi facilitated protein clearance in the

two dRTA mutant cells[31,53] as noted in other studies. In one such study, treatment of SH-SY5Y cells with FCCP and nigericin also acidified intracellular pH and triggered autophagy and mitophagy[31]. Similarly, acid loading in proximal tubular cells under chronic metabolic acidosis showed increased autophagic flux and mitophagy[60]. These findings are in line with our results and establish a link between altered autophagy flux and the alkaline pHi of dRTA variant cells. Overall, our study provides one pathway (altered pHi) by which dRTA may arise. However, different variants induce different degree of functional defects as seen in **Figure 1F** & **G**. The kAE1 R295H, the only reported amino acid substitution in the amino-terminal cytosol causing dRTA, does not affect the transporter's function or pHi. Therefore, this variant may cause dRTA via a different pathway, for example defective protein-protein interactions, than transport-defective S525F or partially inactive R589H variants.

In conclusion, our study established a strong relationship between the expression of defective kAE1 proteins, reduced mitochondrial activity, decreased autophagy and impaired protein degradative flux. Whether this abnormal degradative pathway explains the premature loss of A-IC will need to be elucidated in further studies.

Acknowledgements

We thank Kristina MacNaughton, Jared Bouchard, Kiera Smith and Hilmar Strickfaden for excellent technical assistance. Imaging experiments were performed at the University of Alberta Faculty of Medicine & Dentistry Cell Imaging Core, RRID:SCR_019200, which receives financial support from the Faculty of Medicine & Dentistry, the University Hospital Foundation, Striving for Pandemic Preparedness – The Alberta Research Consortium, and Canada Foundation for Innovation (CFI) awards to contributing investigators. Services were provided by the University of Alberta Faculty of Medicine & Dentistry Workshop, RRID:SCR_019181, which receives financial support from the Faculty of Medicine & Dentistry.

Disclosure and competing interests statement

The authors have no competing interest to declare.

Funding

This study was funded by the Canadian Institutes of Health Research (PJT#168871) and the Kidney Foundation of Canada (2020KHRG-666615) to E.C, by a grant from the Deutsche Forschungsgemeinschaft to M.J.S. (IRTG 1830), and operating funds from Natural Sciences and Engineering Research Council of Canada (RGPIN-2018-05783) and the Canadian Institutes of Health Research (PS#165816) to N.T. G.E. received a Graduate Student Engagement Scholarship, a Faculty of Medicine and Dentistry Delnor Scholarship and a Faculty of Medicine and Dentistry 75th Anniversary award. M.R. received a Sir Frederick Banting and Dr. Charles Best Canada Graduate Scholarship-Master's (CGS-M) from the Canadian Institutes of Health Research; Walter H. Johns Graduate Fellowship; a University of Alberta Faculty of Medicine and Dentistry/Alberta Health Services Graduate Student

423 Recruitment Studentship (GSRS) and an Alberta Graduate Excellence Scholarship (AGES).
424 A.K.M.S.U. received an NSERC CREATE graduate studentship. F.C. was supported by a
425 Discovery Grant to E.C. from the Natural Sciences and Engineering Research Council
426 (RGPIN-2017-06432), and was awarded a Graduate Recruitment scholarship from the
427 University of Alberta. S.M.A.H. received a PhD scholarship from the DAAD (Deutscher
428 Akademischer Austauschdienst).

429

430

References

1. Giglio, S., Montini, G., Trepiccione, F., Gambaro, G. & Emma, F. Distal renal tubular acidosis: a systematic approach from diagnosis to treatment. *Journal of Nephrology* **34**, 2073–2083 (2021).

2. Escobar, L. I. *et al.* Mutations in ATP6V1B1 and ATP6V0A4 genes cause recessive distal renal tubular acidosis in Mexican families. *Mol. Genet. Genomic Med.* **4**, 303–311 (2016).

3. Rungroj, N. *et al.* Distal renal tubular acidosis caused by tryptophan-aspartate repeat domain 72 (WDR72) mutations. *Clin. Genet.* **94**, 409–418 (2018).

4. Enerbäck, S. *et al.* Acidosis and Deafness in Patients with Recessive Mutations in FOXI1. *J. Am. Soc. Nephrol.* **29**, 1041–1048 (2018).

5. Toye, A. M., Banting, G. & Tanner, M. J. A. Regions of human kidney anion exchanger 1 (kAE1) required for basolateral targeting of kAE1 in polarized kidney cells: Mis-targeting explains dominant renal tubular acidosis (dRTA). *J. Cell Sci.* **117**, 1399–1410 (2004).

6. Kollert-Jons, A., Wagner, S., Hubner, H., Appelhans, H. & Drenckhahn, D. Anion exchanger 1 in human kidney and oncocytoma differs from erythroid AE1 in its NH2 terminus. *Am J Physiol* **265**, F813–F821 (2023).

7. Nuiplot, N. *et al.* Transmembrane protein 139 (TMEM139) interacts with human kidney isoform of anion exchanger 1 (kAE1). *Biochem. Biophys. Res. Commun.* **463**, 706–711 (2015).

8. Wu, F. *et al.* Anion Exchanger 1 Interacts with Nephrin in Podocytes. *J. Am. Soc. Nephrol.* **21**, 1456–1467 (2010).

9. Cordat, E. & Reithmeier, R. A. F. Structure, function, and trafficking of SLC4 and SLC26 anion transporters. *Curr. Top. Membr.* **73**, 1–67 (2014).

10. Sawasdee, N. *et al.* Trafficking defect of mutant kidney anion exchanger 1 (kAE1) proteins associated with distal renal tubular acidosis and Southeast Asian ovalocytosis. *Biochem. Biophys. Res. Commun.* **350**, 723–730 (2006).

11. Cheung, J. C., Cordat, E. & Reithmeier, R. A. F. Trafficking defects of the Southeast Asian ovalocytosis deletion mutant of anion exchanger 1 membrane proteins. *Biochem. J.* **392**, 425–434 (2005).

12. Tang, X., Guo, X. & Gao, J. A Novel Compound Heterozygous Mutation in SLC4A1 Gene Causing Severe Hereditary Spherocytosis and Distal Renal Tubular Acidosis. *Indian Journal of Pediatrics* **87**, 233–234 (2020).

13. Ribeiro, M. L. *et al.* Severe hereditary spherocytosis and distal renal tubular acidosis associated with the total absence of band 3. *Blood* **96**, 1602–1604 (2000).

14. Toye, A. M. *et al.* Band 3 Courcouronnes (Ser667Phe): A trafficking mutant differentially rescued by wild-type band 3 and glycophorin A. *Blood* **111**, 5380–5389 (2008).

15. Chang, Y. H. *et al.* Compound mutations in human anion exchanger 1 are associated with complete distal renal tubular acidosis and hereditary spherocytosis. *Kidney Int* **76**, 774–783 (2009).

16. Khositseth, S. *et al.* Tropical distal renal tubular acidosis: clinical and epidemiological studies in 78 patients. *QJM* **105**, 861–877 (2012).

17. Cordat, E. Unraveling trafficking of the kidney anion exchanger 1 in polarized MDCK epithelial cells. *Biochem. Cell Biol.* **84**, 949–959 (2006).

18. Mumtaz, R. *et al.* Intercalated Cell Depletion and Vacuolar H+-ATPase Mistargeting in an Ae1 R607H Knockin Model. *J. Am. Soc. Nephrol.* **28**, 1507–1520 (2017).

19. Festa, B. P. *et al.* Impaired autophagy bridges lysosomal storage disease and epithelial dysfunction in the kidney. *Nat. Commun.* **9**, (2018).

20. Keskanokwong, T. *et al.* Interaction of Integrin-linked Kinase with the Kidney Chloride/Bicarbonate Exchanger, kAE1. *J. Biol. Chem.* **282**, 23205–23218 (2007).

21. Duangtum, N. *et al.* Human kidney anion exchanger 1 interacts with kinesin family member 3B (KIF3B). *Biochem. Biophys. Res. Commun.* **413**, 69–74 (2011).

22. Sawasdee, N. *et al.* Human kidney anion exchanger 1 interacts with adaptor-related protein complex 1 μ1A (AP-1 mu1A). *Biochem. Biophys. Res. Commun.* **401**, 85–91 (2010).

23. Su, Y. *et al.* Glyceraldehyde 3-phosphate dehydrogenase is required for band 3 (anion exchanger 1) membrane residency in the mammalian kidney. *Am J Physiol Ren. Physiol* **300**, 157–166 (2011).

24. Sorrell, S. L., Golder, Z. J., Johnstone, D. B. & Karet Frankl, F. E. Renal peroxiredoxin 6 interacts with anion exchanger 1 and plays a novel role in pH homeostasis. *Kidney Int.* **89**, 105–112 (2016).

25. Bertocchio, J. P. *et al.* Red Blood Cell AE1/Band 3 Transports in Dominant Distal Renal Tubular Acidosis Patients. *Kidney Int. Reports* **5**, 348–357 (2020).

26. Mungara, P. *et al.* Urinary Sodium Wasting and Disrupted Collecting Duct Function in Mice with dRTA-Causing SLC4A1 Mutations. *bioRxiv* 2024.08.21.608692 (2024). doi:10.1101/2024.08.21.608692

27. Zhou, C. *et al.* Monitoring autophagic flux by an improved tandem fluorescent-tagged LC3 (mTagRFP-mWasabi-LC3) reveals that high-dose rapamycin impairs autophagic flux in cancer cells. *Autophagy* **8**, 1215–26 (2012).

28. Kimura, S., Noda, T. & Yoshimori, T. Dissection of the Autophagosome Maturation Process by a Novel Reporter Protein, Tandem Fluorescent-Tagged LC3. *Autophagy* **3**, 452–460 (2007).

29. Mizushima, N. A brief history of autophagy from cell biology to physiology and

disease. *Nat. Cell Biol.* **20**, 521–527 (2018).

30. Hu, M., Zhou, N., Cai, W. & Xu, H. Lysosomal solute and water transport. *J. Cell Biol.* **221**, 1–14 (2022).

31. Berezhnov, A. V. *et al.* Intracellular pH Modulates Autophagy and Mitophagy. *J. Biol. Chem.* **291**, 8701–8708 (2016).

32. Button, R. W., Roberts, S. L., Willis, T. L., Oliver Hanemann, C. & Luo, S. Accumulation of autophagosomes confers cytotoxicity. *J. Biol. Chem.* **292**, 13599 (2017).

33. de Araujo, M. E. G., Liebscher, G., Hess, M. W. & Huber, L. A. Lysosomal size matters. *Traffic* **21**, 60–75 (2020).

34. Ratto, E. *et al.* Direct control of lysosomal catabolic activity by mTORC1 through regulation of V-ATPase assembly. *Nat. Commun.* **13**, 1–15 (2022).

35. Jonckheere, A. I., Smeitink, J. A. M. & Rodenburg, R. J. T. Mitochondrial ATP synthase: Architecture, function and pathology. *J. Inherit. Metab. Dis.* **35**, 211–225 (2012).

36. Yang, M. *et al.* Mutations and clinical characteristics of dRTA caused by SLC4A1 mutations: Analysis based on published patients. *Front. Pediatr.* **11**, 1077120 (2023).

37. Deejai, N. *et al.* Impaired trafficking and instability of mutant kidney anion exchanger 1 proteins associated with autosomal recessive distal renal tubular acidosis. *BMC Med. Genomics* **15**, 1–12 (2022).

38. Chu, C. Y. S., King, J. C., Berrini, M., Alexander, R. T. & Cordat, E. Functional Rescue of a Kidney Anion Exchanger 1 Trafficking Mutant in Renal Epithelial Cells. *PLoS One* **8**, (2013).

39. Dhingra, A., Alexander, D., Reyes-Reveles, J., Sharp, R. & Boesze-Battaglia, K. Microtubule-associated protein 1 light chain 3 (LC3) isoforms in RPE and retina. *Adv.*

Exp. Med. Biol. **1074**, 609–616 (2018).

40. Huang, X. *et al.* S-acylation of p62 promotes p62 droplet recruitment into autophagosomes in mammalian autophagy. *Mol. Cell* **83**, 3485-3501.e11 (2023).

41. Yamamoto, T. *et al.* High-fat diet-induced lysosomal dysfunction and impaired autophagic flux contribute to lipotoxicity in the kidney. *J. Am. Soc. Nephrol.* **28**, 1534–1551 (2017).

42. Lee, W. K. *et al.* Initial autophagic protection switches to disruption of autophagic flux by lysosomal instability during cadmium stress accrual in renal NRK-52E cells. *Arch. Toxicol.* **91**, 3225–3245 (2017).

43. Brown, C. N. *et al.* Surgical procedures suppress autophagic flux in the kidney. *Cell Death Dis.* **12**, (2021).

44. Mizushima, N., Ohsumi, Y. & Yoshimori, T. Autophagosome formation in mammalian cells. *Cell Struct. Funct.* **27**, 421–429 (2002).

45. Klionsky, D. J. *et al.* Guidelines for the use and interpretation of assays for monitoring autophagy. *Autophagy* **8**, 445–544 (2012).

46. Liu, F. *et al.* Cathepsin B: The dawn of tumor therapy. *Eur. J. Med. Chem.* **269**, 116329 (2024).

47. Höhne, M. *et al.* Single-nephron proteomes connect morphology and function in proteinuric kidney disease. *Kidney Int.* **93**, 1308–1319 (2018).

48. Ballabio, A. & Gieselmann, V. Lysosomal disorders: From storage to cellular damage. *Biochim. Biophys. Acta - Mol. Cell Res.* **1793**, 684–696 (2009).

49. Eskelinen, E. L. Roles of LAMP-1 and LAMP-2 in lysosome biogenesis and autophagy. *Mol. Aspects Med.* **27**, 495–502 (2006).

50. Thornell, I. M. & Bevensee, M. O. Regulators of Slc4 bicarbonate transporter activity. *Front. Physiol.* **6**, (2015).

556 51. Zhang, Q. *et al.* The structural basis of the pH-homeostasis mediated by the
557 Cl−/HCO3− exchanger, AE2. *Nat. Commun.* **14**, (2023).
558 52. Romero, M. F., Chen, A. P., Parker, M. D. & Boron, W. F. The SLC4 family of
559 bicarbonate (HCO3-) transporters. *Mol. Aspects Med.* **34**, 159–182 (2013).
560 53. Korolchuk, V. I. *et al.* Lysosomal positioning coordinates cellular nutrient responses.
561 *Nat. Cell Biol.* **13**, 453–462 (2011).
562 54. Heuser, J. Changes in lysosome shape and distribution correlated with changes in
563 cytoplasmic pH. *J. Cell Biol.* **108**, 855–864 (1989).
564 55. Xu, T., Su, H., Ganapathy, S. & Yuan, Z. M. Modulation of autophagic activity by
565 extracellular pH. *Autophagy* **7**, 1316–1322 (2011).
566 56. Mizushima, N. & Komatsu, M. Autophagy: Renovation of Cells and Tissues. *Cell* **147**,
567 728–741 (2011).
568 57. Schütt, F., Aretz, S., Auffarth, G. U. & Kopitz, J. Moderately reduced ATP levels
569 promote oxidative stress and debilitate autophagic and phagocytic capacities in human
570 RPE cells. *Investig. Ophthalmol. Vis. Sci.* **53**, 5354–5361 (2012).
571 58. Nguyen, T. T. *et al.* Intracellular alkalinization by phosphate uptake via type III
572 sodium-phosphate cotransporter participates in high-phosphate-induced mitochondrial
573 oxidative stress and defective insulin secretion. *FASEB J.* **30**, 3979–3988 (2016).
574 59. Lyons, J. C., Kim, G. E. & Song, C. W. Modification of intracellular pH and
575 thermosensitivity. *Radiat. Res.* **129**, 79–87 (1992).
576 60. Namba, T. *et al.* Autophagic clearance of mitochondria in the kidney copes with
577 metabolic acidosis. *J. Am. Soc. Nephrol.* **25**, 2254–2266 (2014).
578
579

Figure Legends

Figure 1. kAE1 R295H, Y413H, S525F and R589H dRTA mutants are either dysfunctional or prematurely degraded. (A) Alpha Fold predicted structure of the kidney isoform of Band 3 anion exchanger 1 (kAE1) with core and gate domains highlighted. The dRTA kAE1 mutation sites are coloured in blue with line extensions detailing specific amino acids mutated. (B) Immunoblot showing expression of kAE1 WT, R295H, Y413H, S525F and R589H and corresponding actin band in mIMCD3 cells treated with and without doxycycline for 24 hrs. Mouse anti-HA antibody was used to detect kAE1-HA, top (open circle) and bottom bands (closed circle) correspond to kAE1 carrying complex and high mannose oligosaccharides, respectively. (C) Immunostaining of kAE1 WT or mutant (red) and β-catenin (green) in polarized mIMCD3 cells. Scale bar = 10 μm. Red = kAE1, Green = ß-Catenin. (D) Immunoblot of cycloheximide (CHX) chase assay with corresponding actin in kAE1 mIMCD3 WT and Y413H cells showing the degradation of kAE1 Y413H after 3hrs CHX incubation. (E) Cartoon depicting the transporter activity and expected changes in pHi in cells expressing kAE1 WT (left) or inactive mutant (right). (F) Graphical representation of intracellular pH (pHi) measurement of mIMCD3 kAE1 WT, R295H, Y413H, S525F and R589H cells. Error bars correspond to mean ± SEM, n = minimum 32. *P<0.05, **P<0.01 using one-way ANOVA followed by a Dunnett's post-hoc test. (G) Rate of intracellular alkalinisation in WT or mutant mIMCD3 cells normalized to WT+ Dox. **** indicates P < 0.0001 using one-way ANOVA followed by a Dunnett's post-hoc test. Error bars correspond to mean ± SEM, n= minimum 4

Figure 2. Autophagy is upregulated in dRTA kAE1 mutants *in vitro* and *in vivo*. (A-C) Representative immunoblots of LC3B and p62 with corresponding actin abundance in kAE1 WT, R295H, S525F and R589H mIMCD3 cells at steady state, under starvation (Starv) or

400 nM Bafilomycin A1 (Baf) treatment. Note that p62 and LC3B were detected on the same blot for panel A and C, therefore the same actin blot is shown for both panels. (D-I) Quantification of all immunoblots showing the ratio of LC3B II to total LC3B and p62. Error bars correspond to mean ± SEM, n= 3-8. * P<0.05, ** P<0.01, *** P<0.005, ****P < 0.001 using one-way ANOVA followed by a Tukey's post-hoc test. Immunoblots (J) and quantification (K, L) of LC3B and p62 abundance in kAE1 R607H KI mouse whole kidney lysates. Error bars correspond to mean ± SEM, n= minimum 5. ***P < 0.005 using one-way ANOVA followed by a Tukey's post-hoc test.

Figure 3. dRTA kAE1 mutants have more alkaline steady-state intracellular pH and altered autophagy flux. (A) Representative immunoblots of cell surface biotinylation experiments in mIMCD3 cells expressing kAE1 WT or mutants (top panels), with control staining of plasma membrane marker Na^+/K^+-ATPase (middle panel) and intracellular marker actin (bottom panel). (B) Quantification of 3 independent cell surface biotinylation experiments. Data are represented by a single representative blot for each variant. N.s., not significant using one-way ANOVA. Error bars correspond to mean ± SEM, n=3. (C) Immunofluorescence staining in eGFP-RFP-LC3 transfected mIMCD3 cells expressing kAE1. GFP = green, RFP = red, kAE1= cyan, nuclei = dark blue (merge only). Scale bar = 2 µm. Graphical representation of number of yellow (autophagosomes) (D) and red (autolysosomes) (E) puncta per cell expressing kAE1. Error bars correspond to mean ± SEM, n= minimum 32. ** P<0.01, *** P<0.005, ****P < 0.001 using one-way ANOVA followed by a Tukey's post-hoc test. (F) Grouped graph of the number of yellow (autophagosomes) and red (autolysosomes) puncta per cell expressing kAE1, respectively. Note that the statistical analysis displayed only compared yellow and red groups for simplification. Error bars correspond to mean ± SEM, n= minimum 32. ** P<0.01, ****P < 0.001 using two-way

ANOVA followed by a Sidak's post-hoc test. (G-I) Immunoblot of LC3B, LAMP1 and actin in kAE1 WT, S525F and R589H mIMCD3 cells at steady state and under chemically reduced intracellular pH conditions. Graphical representation of the ratio of LC3B II to total LC3B ratio (J) or LAMP 1 (K) at steady state versus at low pHi in mIMCD3 kAE1 WT, S525F and R589H. Black circles indicate steady state cells and triangles indicate low pHi cells. Error bars correspond to mean ± SEM, n= 3. ** indicates P<0.01 using two-way ANOVA followed by a Sidak's post-hoc test.

Figure 4. dRTA kAE1 mutants have bigger or more lysosomes than WT *in vitro* and *in vivo*. (A) Immunofluorescence images of kAE1 WT, S525F and R589H mIMCD3 cells incubated with Magic Red substrate for 1hr at 37°C in the dark. Green = kAE1, magenta = active lysosomes, blue = nuclei. Scale bar =16 µm. (B) Graphical representation of number and size of active lysosomes per cell. Error bars correspond to mean ± SEM, n= minimum 30. **** P<0.0001 using one-way ANOVA followed by Tukey's post-hoc test. Immunofluorescence images of LAMP 1 and ß1 ATPase in kidney cortex (C) or medulla (E) from kAE1 WT and R607H KI mice. Blue = nuclei, magenta = LAMP 1 (lysosomes), Yellow = ß1 ATPase, light blue "G" indicates the location of a glomerulus. Scale bar = 8µm. Graphical representation of the number and volume of LAMP1 vesicles in ß1 ATPase positive cells in the kidney cortex (D) or medulla (F) of WT or R607H KI mice. Error bars correspond to mean ± SEM, n= 60. **** P<0.001 using Student's t-test.

Figure 5. dRTA kAE1 mutant cells have lower ATP production rate and abnormal mitochondrial content. Oxygen consumption rate (OCR) (A) and Extra Cellular Acidification Rate (ECAR) (B) of empty vector (EV) transfected cells, kAE1 WT, S525F or R589H mIMCD3 cells analyzed in a Seahorse XFe96 Extracellular Flux Analyzer with the

ATP Rate Assay Test Kit. All cell lines, including EV transfected cells, were incubated with doxycycline, to eliminate a potential effect of doxycycline on measurements. (C) Graphical representation of the combination of ATP production rates from mitochondrial respiration (mitoATP) and glycolysis (glycoATP) of kAE1 WT, S525F and R589H mIMCD3 cells measured in real-time following sequential injections of oligomycin and Rotenone +Antimycin A. Error bars correspond to mean ± SEM, n= minimum. * $p < 0.05$, ****$p < 0.0001$ using one-way ANOVA followed by Tukey's post-hoc test. Graphical representations of mitochondrial respiration (D) and glycolytic ATP production (E) in kAE1 WT, S525F and R589H mIMCD3 cells. Error bars correspond to mean ± SEM, n= minimum 8. **P<0.01, ****$p < 0.0001$ using one-way ANOVA followed by Tukey's post-hoc test. (F) Immunofluorescence staining of TOM 20 and kAE1 in kAE1 WT, S525F and R589H mIMCD3 cells. Blue = nuclei, Magenta = TOM 20, Green = kAE1. Scale bar = 8 µm. (G) Graphical representation of total TOM 20 fluorescence intensity per cell expressing kAE1. Error bars correspond to mean ± SEM, n= minimum 40. ***$p < 0.001$, ****$p < 0.0001$ using one-way ANOVA followed by Tukey's post-hoc test. Immunofluorescence images of TOM 20 and ß1 ATPase in kidney cortex (H) or medulla (J) of kAE1 R607H WT and KI mice exposed to a salt depleted diet with an acid challenge[26]. Blue = nuclei, magenta = TOM 20 (mitochondria), Yellow = ß1 ATPase, light blue "G" indicates the location of a glomerulus. Scale bar = 8µm. Graphical representation of the total TOM 20 fluorescence intensity in ß1 ATPase positive cells in the cortex (I) or medulla (K) of the kidney. Error bars correspond to mean ± SEM, n= 90. * $p < 0.05$, ****$p < 0.0001$ using Student's t-test.

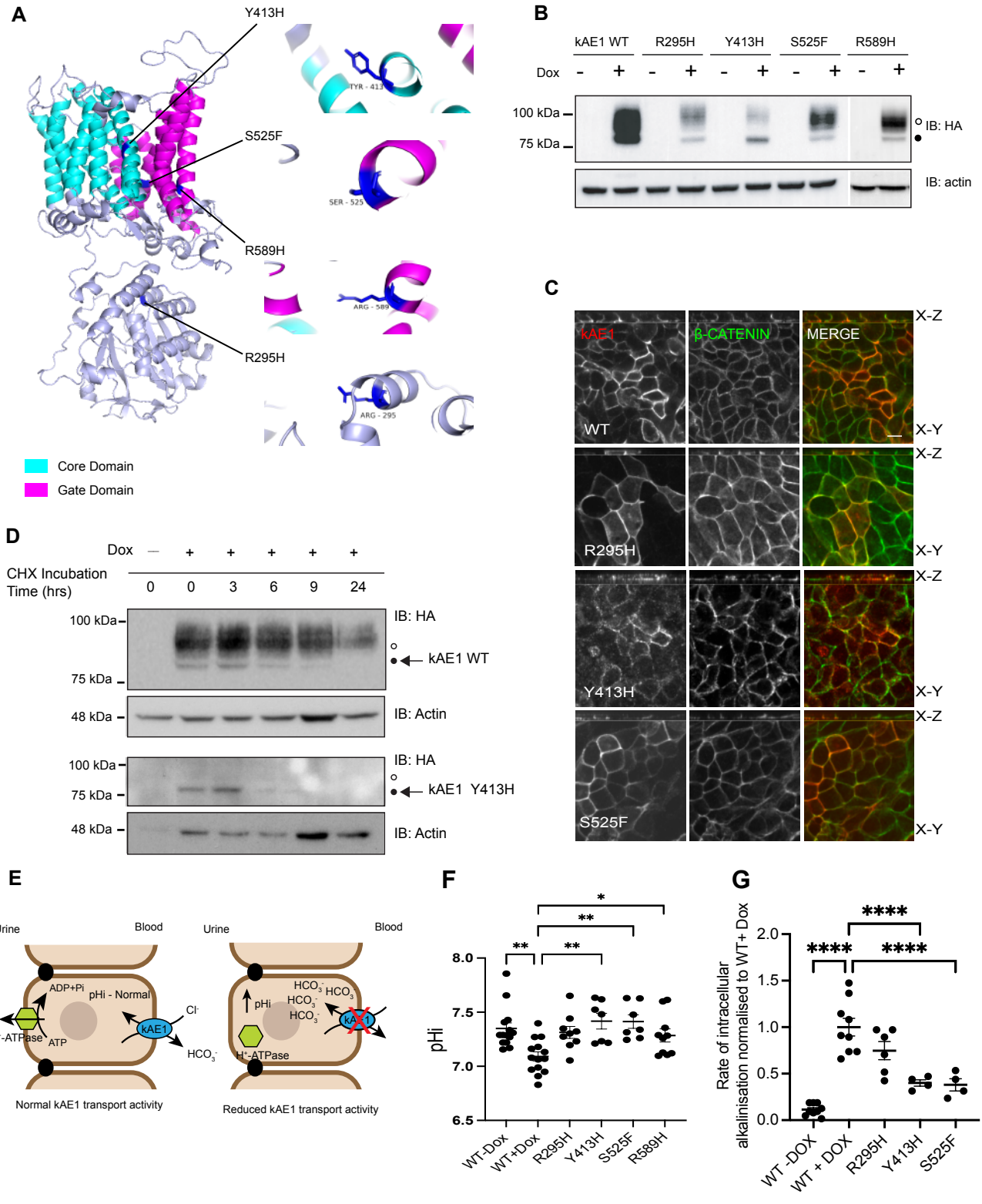

Figure 1 Essuman et al.

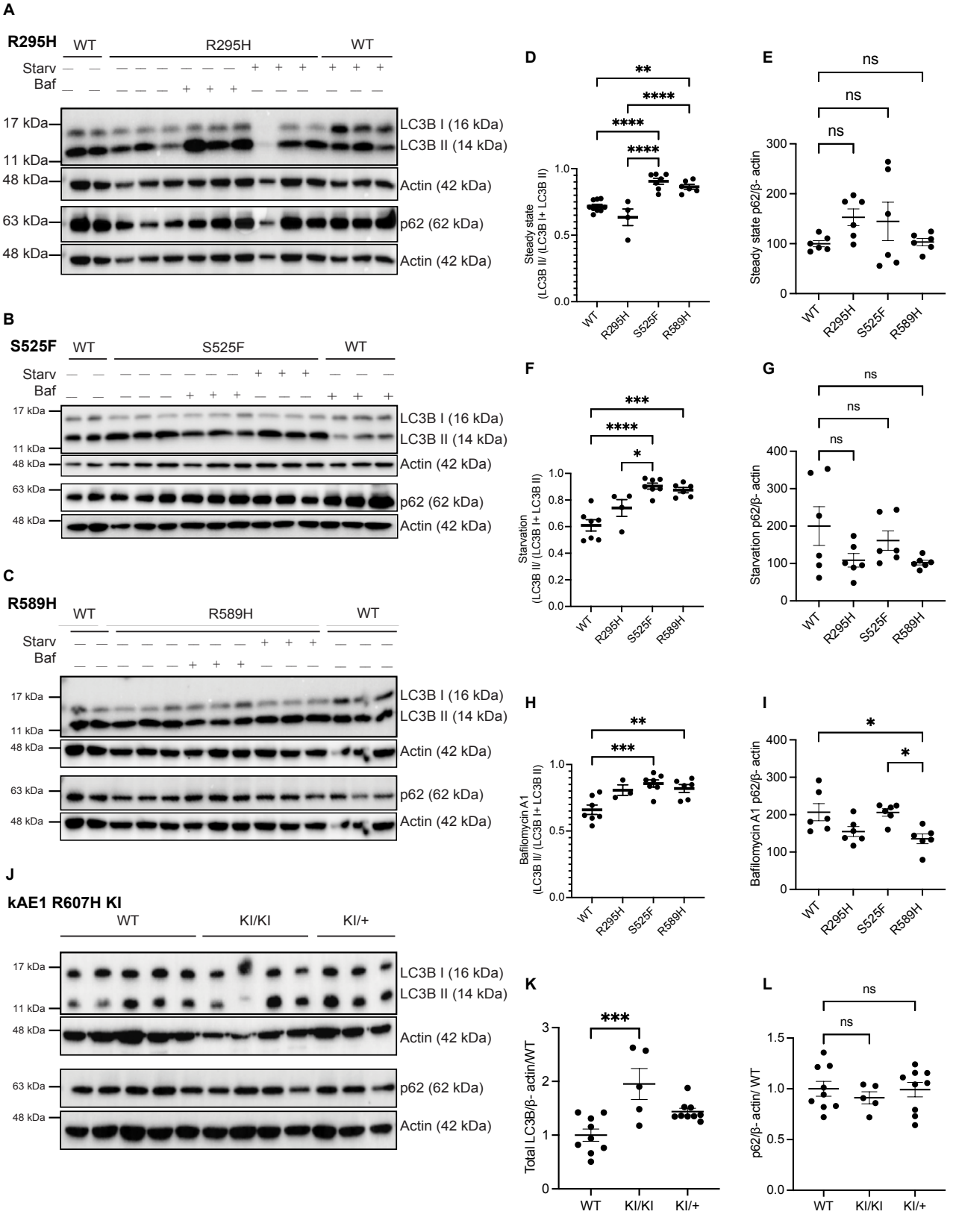

Figure 2 Essuman et al.

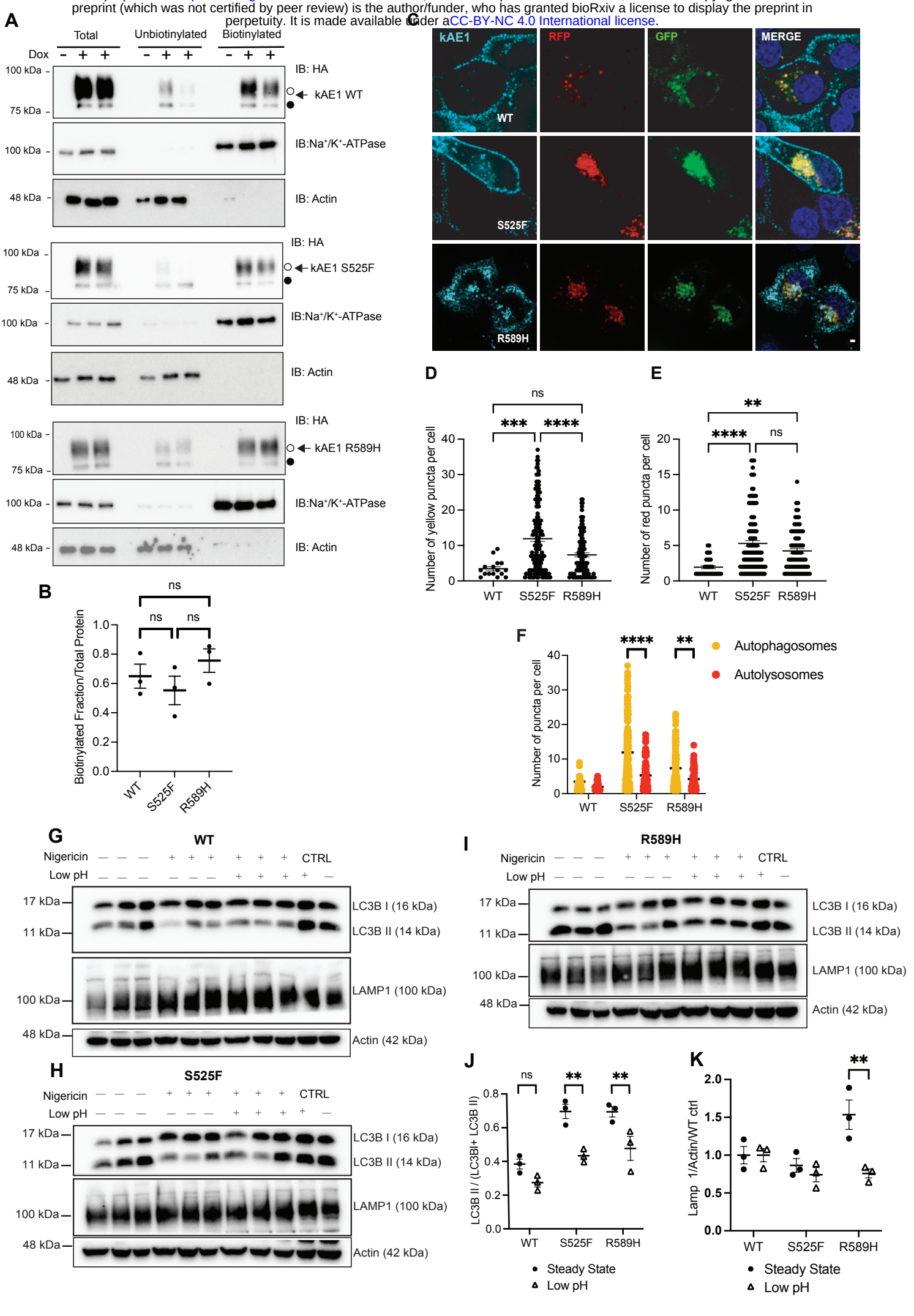

Figure 3 Essuman et al.

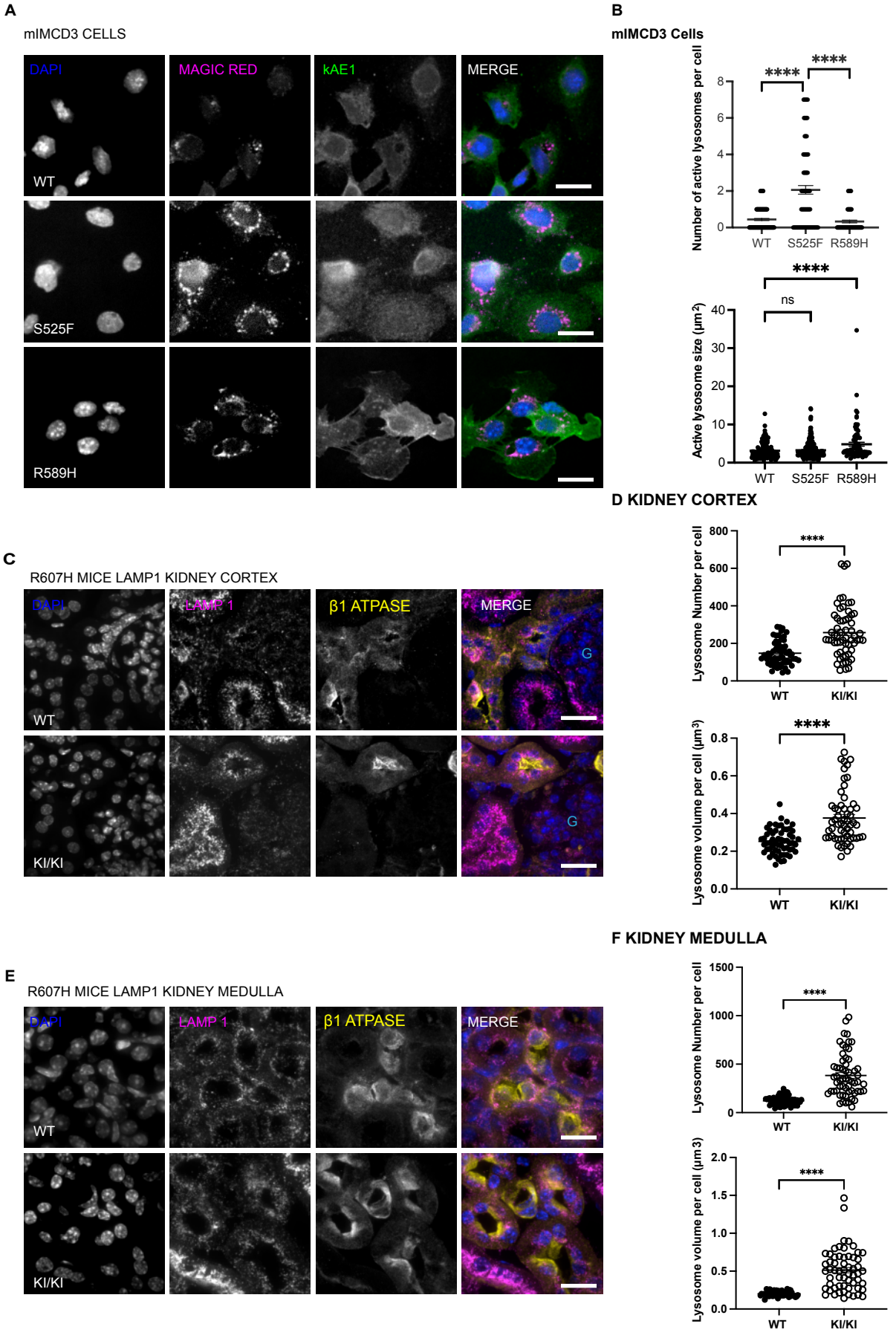

Figure 4 Essuman et al.

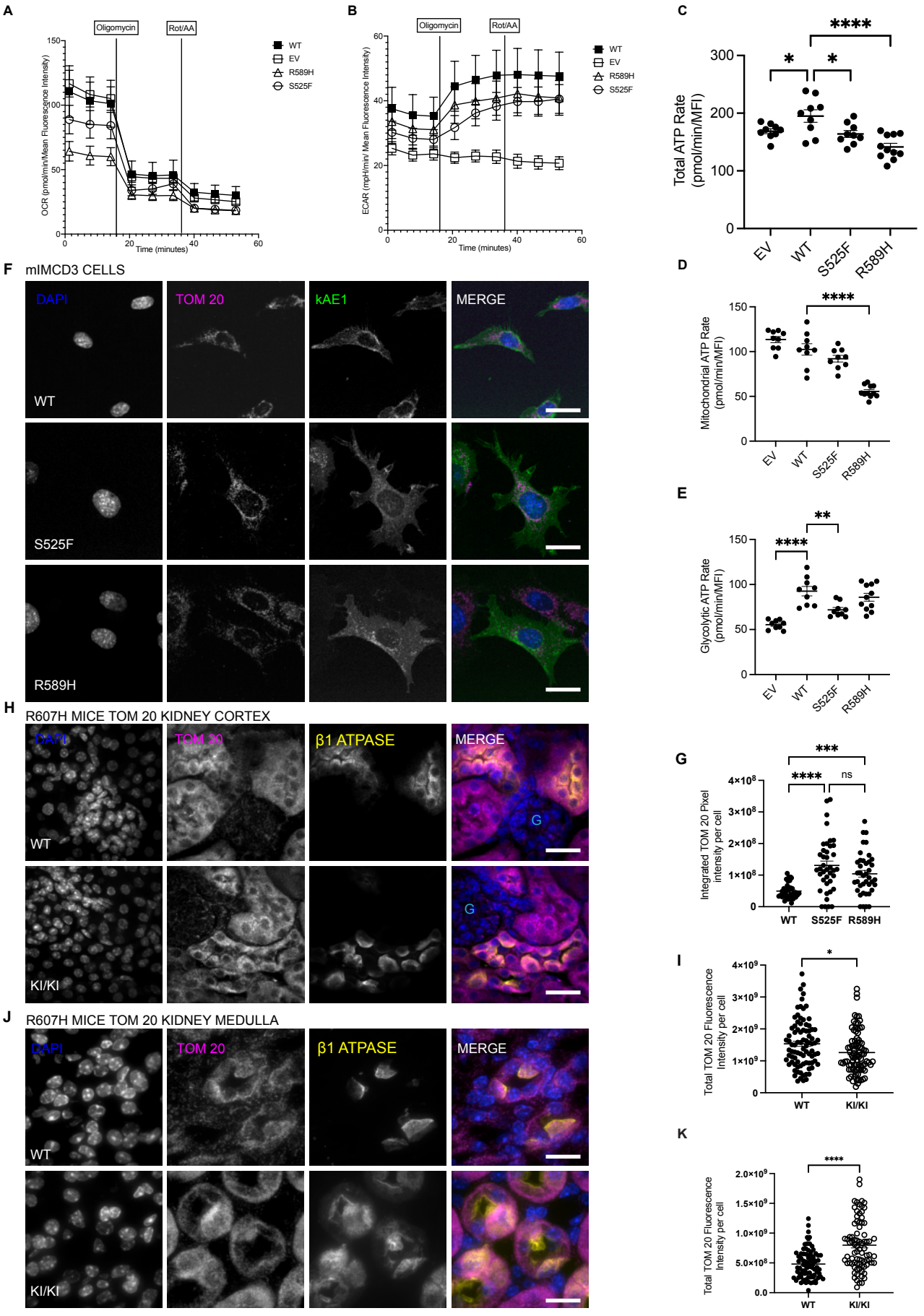

Figure 5 Essuman et al.

SLC4A1 MUTATIONS THAT CAUSE DISTAL RENAL TUBULAR ACIDOSIS ALTER CYTOPLASMIC PH AND IMPAIR CELLULAR AUTOPHAGY

Grace Essuman[1], Midhat Rizvi[1], Ensaf Almomani[6], Shahid AKM Ullah[1,5], Sarder M. A. Hasib[3], Forough Chelangarimiyandoab[1], Priyanka Mungara[1], Manfred J. Schmitt[3], Rosa Vargas-Poussou[2], Nicolas Touret[4] & Emmanuelle Cordat[1*]

Supplementary Material

Material and Methods

Ethics Approval

This study was conducted in accordance with all national and institutional animal care guidelines and approved by the University of Alberta's Animal Care and Use Committee (AUP #1277).

Antibodies and chemicals

Mouse anti-HA antibody (hemagglutinin, Biolegend, formerly Covance), mouse anti-β-actin antibody (Sigma Aldrich or anti -β-actin HRP clone 2F1-1 Biolegend cat#643807), mouse anti-LC3B antibody (Cell Signaling), mouse anti- IVF 12s antibody (Developmental Studies Hybridoma Bank), rat anti-ATP6V1B1 antibody (BiCell #20901), rabbit anti- mTOR antibody and phospho mTOR antibody (Cell Signaling), Rabbit anti-4E-BP1 antibody and phospho 4E-BP1 (Ser65) antibody (Cell Signaling), mouse anti-p62 antibody (Abcam), mouse anti-p53 antibody (Cell Signalling), rabbit anti-Cleaved caspase 3 antibody (Cell Signalling), mouse monoclonal anti Na^+/K^+-ATPase H-3 antibody (Santa Cruz Biotechnology, Dallas, TX), goat anti-mouse antibody horseradish peroxidase conjugated (HRP) (Cell Signaling Technology), Cy3-conjugated donkey anti-mouse antibody, anti-rabbit and anti-goat antibodies (Jackson Immunoresearch), X-tremeGENE HP DNA transfection reagent (Roche), Seahorse XFe consumables (Agilent).

Cell Lines, Transfections and Viral Infection

Mouse inner medullary collecting duct (mIMCD) cells (ATCC# CRL2123) were used for preparing kAE1 wild type and mutant cell lines. The pLVX TRE3G kAE1 construct was generated from the shuttling of human kAE1 cDNA with an external hemagglutinin (HA) epitope in position 557 (on eAE1) into pLVX-TRE3G plasmid (Clontech)[1]. This construct encodes a protein described as kAE1 throughout this paper. The kAE1 S525F and R589H mutants were generated with Q5 site-directed mutagenesis. All plasmids were introduced into the mIMCDs using a viral single shot packaging kit (Clontech).

Mouse intercalated cell isolation and tissue homogenate preparation

Kidney tissue homogenates were prepared as previously described[2]. Briefly, after decapsulation, freshly dissected kidneys were homogenized in cold lysis buffer (0.3 M Sucrose, 25 mM Imidazole, 1mM EDTA, 8.5 µM Leupeptin, 1 mM PMSF), and vortexed over one hour every 15 min. Thie homogenates were then centrifuged at 14000 rpm for 15 minutes at 4 °C prior to measurement of protein concentration by Bicinchoninic Acid Protein Assay. Primary intercalated cells were prepared from homozygous kAE1 R607H transgenic mice. After cardiac

perfusion with PBS, heparin, and collagenase B (Sigma Aldrich), kidneys were homogenized by MACS dissociation and intercalated cells enriched using CD 117 magnetic sorting (Miltenyi Biotec) as previously described[3]. During the selection, intercalated cells were kept in MACS buffer (PBS, 2mM EDTA and and 0.5 % FBS). Cells were lysed with RIPA lysis buffer (2 mM EDTA, 2 % Deoxycholate, 0.3 M NaCl, 20 mM Tris/HCl pH 7.5, 2 % Triton X-100, 0.2 % SDS, pH 7.4), supplemented with complete EDTA-free protease inhibitors, and PhoSTOP phosphatase inhibitor (Roche), PMSF, pepstatin, leupeptin and aprotinin. An aliquot was saved for bicinchoninic acid assay to determine protein concentration and remaining lysates were kept in Laemmli buffer at -20°C for immunoblotting.

Bicarbonate transport assay

This assay has been previously described[4]. Briefly, confluent kAE1 WT-HA or mutant mIMCDs cells grown on coverslips were incubated with 1 μg/ml doxycycline (Sigma-Aldrich) for 18 - 24 hours at 37°C to induce kAE1 expression. They were then incubated with 2',7'-Bis-(2-Carboxyethyl)-5-(and-6)-Carboxyfluorescein, Acetoxymethyl Ester (BCECF – AM, Thermo Scientific), a fluorophore which excites at 440 and 490 nm and emits 510 nm wavelength for 30 minutes at 37°C. Using a fluorometer from Photon Technologies International (PTI) (London, Ontario, Canada), coverslips were perfused with NaCl-based Ringer's buffer (5 mM glucose, 5 mM potassium gluconate, 1 mM calcium gluconate, 1 mM magnesium sulfate, 10 mM HEPES, 2.5 mM sodium dihydrogen phosphate, 25 mM sodium bicarbonate,140 mM sodium chloride) for 5 to 10 minutes. Once stable, initial fluorescence (corresponding to steady -state pHi)) was recorded for the first 30 seconds before switching to chloride-free containing sodium gluconate based Ringer's buffer of same osmolality. BCECF fluorescence was calibrated by perfusing cells with different pH buffers (6.5, 7, 7.5) in the presence of 10 μM nigericin. The Ringer's buffers were continuously bubbled with an air: CO2 mixture (19:1), providing 5 % CO2. Transport rates of the cells were determined by linear regression of the initial fluorescence variations (over the first 60 seconds), normalized to pH calibration measurements. All measurements were done using PTI FelixGX software.

Cell Treatments and immunoblotting

For autophagy experiments kAE1 WT or mutant cells were seeded to 70 % confluency on 10 cm culture plates and treated with 1 μg/ml doxycycline (Sigma-Aldrich) for 48 hours. Cells were then either treated with 400 nM bafilomycin A1 for four hours to inhibit autophagy or with Hanks balanced salt solution (HBSS, Gibco) to starve cells and induce autophagy or given no treatment. To chemically modify pHi of cells, 90 – 100 % confluent cells were treated with 1μg/ml of doxycycline (Sigma-Aldrich) overnight. Cells were then incubated in Ringers' buffer with pH 6.6, supplemented with 0.03 μM nigericin with a final potassium concentration of 168mM for two hours at 37ºC. Steady-state cells were incubated in normal pH media without nigericin prior to lysis. Under treated conditions, pHi was similar to pHe (**Supplementary Figure 1**). Cells were lysed with RIPA lysis buffer (1% deoxycholate, 1mM EDTA, 0.15 M NaCl, 0.1% SDS, 10 mM TRIS/HCL (pH 7.5), 1% Triton X-100) with phosphatase inhibitors (cat. no. 04906837001; Roche PhosSTOP) and protease inhibitors (cat. no. 04693159001; Roche Complete Tablets, Mini EDTA-free) and stored at −20 °C with or without 2x Laemmli buffer. The aliquot without Laemmli buffer was used for a bicinchoninic acid (BCA) assay to determine protein concentration. Following the BCA, 10 - 30 μg of total protein was loaded on SDS-PAGE gels. Proteins were transferred to PVDF membranes and antibodies listed above were used for

detecting the proteins of interest. Primary antibodies were diluted in 1 % milk and incubated on membranes overnight at 4 °C followed by secondary antibodies linked with horseradish peroxidase (HRP) for one hour at room temperature. Protein detection was done with the Enhanced Chemiluminescence reagent (ECL Prime, Invitrogen), and a BioRad Imager. The ImageLab software (BioRad) was utilized for the quantification of relative band intensities.

Cell Surface Biotinylation assay

mIMCD3 cells stably expressing kAE1 WT, S525F or R589H were seeded to 70-80% confluency. The cells were incubated with sulfo-N-hydroxysuccinimide-SS-biotin (Thermo cat.# 21331) (1.5 mg/ml in ice-cold PBS) for an hour at 4°C, quenched with 100mM glycine and lysed with RIPA lysis buffer, supplemented with complete EDTA-free protease inhibitors, and PhoSTOP phosphatase inhibitor (Roche), PMSF, pepstatin, leupeptin and aprotinin. Total protein levels were measured by BCA, and an aliquot was saved as "Total" fraction. 450 µg of each lysate was subsequently incubated with 100 µl streptavidin slurry beads for 1 h on a rocker at 4°C. Following centrifugation, the supernatant was collected, and an aliquot kept as the "unbiotinylated" fraction. After six washes, the beads were resuspended in 50 µl of 2X Laemmli buffer and incubated at room temperature for 30 min. The eluted biotinylated proteins were subsequently collected by centrifugation ("Biotinylated" fraction). The biotinylated fraction (45 µl) was loaded on SDS-PAGE gel for immunoblot analysis along with 3 µg of the Total fraction and a matched volume of unbound fraction per well. In addition to anti-HA antibody, the blots were probed for actin to ensure cell membrane integrity was intact during the biotinylation procedure, and for Na^+/K^+-ATPase as cell surface control.

Magic Red Assay

80 % confluent kAE1 WT or mutant mIMCD3 cells were treated with 1 µg/ml doxycycline (Sigma-Aldrich) for 48 hours to induce kAE1 expression. Different treatments including: a 4-hour incubation with 400 nM bafA1 to inhibit autophagy, a 2-hour starvation in HBSS to induce autophagy or no treatment (steady state) were applied. Cells were then incubated with 1 % Magic Red reagent (ImmunoChemistry Technologies) in DMEM-F12 medium at 37°C in the dark for 30-60 minutes. Cells were then fixed with 4 % PFA, quenched with 100 mM glycine, permeabilized with 0.2 % Triton X-100, blocked with 1 % BSA and incubated with mouse anti-HA primary antibody and donkey anti-mouse Alexa fluor 488 conjugated secondary antibody for 30 mins each. Cells were then incubated with 4′,6-diamidino-2-phenylindole (DAPI) for 5 mins before mounting using DAKO Mounting Medium (Agilent Technologies). A WaveFX confocal microscope was used to image the slides, and the images were analyzed blindly using the Fiji software.

Autophagy flux Assay

kAE1 WT-HA or mutant mIMCD3 cells seeded to 70 % confluency in a 6-well plate on coverslips were transiently transfected with the eGFP-RFP-LC3 cDNA construct (kind gift from Dr. Goping, Department of Biochemistry, University of Alberta) using the X-tremeGENE HP DNA transfection reagent (Roche). Four hours after transfection, the cells were incubated with 1 µg/ml doxycycline for 48 hours at 37°C to induce kAE1 expression. Following this incubation, cells were incubated with blocking medium, mouse anti-HA primary antibody (1:200) and donkey anti-mouse Alexa fluor 649 (Jackson ImmunoResearch). Hoescht stain (ImmunoChemistry Technologies) was used to stain cellular nuclei. A WaveFX confocal

microscope together with the Velocity and Fiji software were used to capture and analyze images.

Assessment of mitochondrial content

kAE1 WT-HA or mutant mIMCD3 cells seeded to 50 % confluency in a 6-well plate on coverslips were incubated with 1 μg/ml doxycycline for 48 hours at 37°C and overnight in complete medium with no antibiotics. Cells were then fixed with 4 % PFA, quenched with 100 mM glycine, permeabilized with 0.2 % Triton X-100, blocked with 1 % BSA and incubated with mouse anti-HA and rabbit anti-TOM 20 primary antibodies and then with donkey anti-mouse Alexa fluor 488 and anti-rabbit Cy3 conjugated secondary antibodies. Cells were then incubated with 4′,6-diamidino-2-phenylindole (DAPI) for 5 mins before mounting using DAKO Mounting Medium (Agilent Technologies). A WaveFX confocal microscope was used to image the slides, and the images were analyzed blindly using the Fiji software.

Metabolic flux analysis

kAE1 WT-HA or mutant mIMCD3 cells were treated with 1 μg/ml doxycycline for 48 hours followed by an overnight incubation in complete media with no antibiotics and cells seeded at 2 x 10^4 cells per well in Seahorse XFe 96 well plates overnight to form a uniform monolayer. On the day of assay, culture medium was replaced with XF DMEM Medium pH 7.4 (103575-100, Agilent Technologies) with glucose (10 mM), pyruvate (1 mM) and L-Glutamine (2 mM) and incubated in a non-CO_2, 37°C incubator for one hour prior to their placement into the XFe96 Analyzer. Using the ATP production rate assay kit (#103592-100, Agilent Technologies) and XF cell Mito Stress Test kit (#103015–100, Agilent Technologies), metabolic indices were obtained from the Seahorse XFe96 Analyzer following manufacturer's procedures previously described[23]. The total ATP rate is the sum of ATP production rate from both glycolysis and oxidative phosphorylation. Glycolysis releases protons in a 1:1 ratio with ATP hence the glycolytic ATP rate is calculated from the glycolytic proton efflux rate (glycoPER). GlycoPER is determined by subtracting respiration linked proton efflux from total proton efflux by inhibiting complex I and III. The empty vector transfected cells provided a control for a potential effect of doxycycline on measurements. Oxygen consumption rate (OCR) and extracellular acidification rate (ECAR) were measured at various time points at basal state followed by injections of oligomycin (1.5 μM) and Rotenone +Antimycin A (0.5 μM).

Tissue Preparation and Immunostaining of kidney sections

Kidneys collected after perfusion were stored in 4 % PFA overnight at 4°C. The PFA solution was switched to 15 % sucrose for 2 hours and then transferred to 30 % sucrose solution overnight at 4°C. Thereafter, kidneys were fixed in O.C.T (Tissue-Tek®) and snap frozen in liquid nitrogen. These tissues were stored at -80°C until cryo-sectioning. Ten (10) micron tissue sections were fixed on a charged glass slide (ThermoFisher) and used immediately or stored at -80°C until immunostaining. For immunostaining, the slices were first air-dried for 20 mins, washed with PBS for 5 minutes and fixed with 4 % PFA for 20 mins at 4°C. The sections were quenched with 100 mM glycine for 15 minutes, permeabilized and blocked with 5 or 10 % serum in 0.2 % Triton in PBS for one hour at room temperature. Slices were incubated in primary antibody diluted in 5 or 10 % serum overnight at 4°C followed by secondary antibody diluted in 5 or 10 % serum for one hour at room temperature. Slices were washed with 0.1 % Tween 20 in PBS and incubated with DAPI for 5 mins at room temperature, mounted with DAKO mounting

medium and sealed. Slides were air-dried and then stored at -20˚C. Note that kidney sections analyzed in **Figure 5H-K** were obtained from mice fed a "salt-depletion with acid load" diet consisting of a low sodium and chloride diet for 8 days, complemented with 0.28 M NH_4Cl with 0.5 % sucrose in drinking water for 6 additional days as previously described[2]. This diet triggered a metabolic acidosis, significantly lower plasma bicarbonate with a more alkaline urine in the homozygous KI mice compared to WT littermates.

Confocal imaging and image analysis

Immunofluorescent imaging was done with a WaveFX confocal microscope (Quorum Technologies, Guelph, Ontario, Canada) powered by a Volocity software (Quorum Technologies, Guelph, Ontario, Canada). Images were taken with 40 X oil immersion objective with z-stacks at 0.5- µm intervals. Quantitative image analysis was performed using the Volocity analysis software or by open-source cell image analysis softwares CellProfiler[5] and Fiji[6].

Image Analysis

Cell profiler was used to analyse TOM20 staining in mIMCD3 cells. After converting the three channel RGB images to grayscale using the split method, we manually outlined each cell in the channel corresponding to kAE1 staining and inputted back into the pipeline. The objects were then converted to a binary image and the TOM20 channel was used as the input channel to measure intensity of TOM20 staining in the manually outlined objects. The raw data including the sum of TOM 20 pixel intensity per cell were then analysed using GraphPad Prism software. A minimum of 30 cells were analysed.

Fiji software was used to analyse images from Magic Red staining and autophagy flux experiment. After each multichannel image was opened and merged in Fiji, the "multi point" tool was used to label all regions of interest. Freehand selection tool was used to manually draw the outline of all selected regions of interest, followed by the "Analyze" command to extract number and size of puncta in pixels. Pixel values were then converted to microns and data analysis was completed using GraphPad Prism. A minimum of 30 cells were analyzed.

Volocity software was used for analysis of kidney sections. From B1 H^+-ATPase-positive single cells cropped from confocal images of medullary or cortical mouse kidney sections, the channel of interest was used to find objects using the "Find objects" command. Refinement within the selection was made based on object size. The minimum object size thresholds were 0.016 μm^2 for LAMP1 puncta and 0.02 μm^2 for TOM20 staining. This was then labelled as "population one". From population one, touching objects were separated using a size guide of 0.02 μm^2 for LAMP 1 puncta only with the "Separate touching objects" function. For TOM20 staining, all RFP positive stain within individual cells were characterized under one mask without separating touching objects. The minimum object size was set to 0.02 μm^2 and everything less than that was considered background staining. The sum of TOM 20 fluorescence intensity per cell was collected and analysed using GraphPad Prism. For LAMP1 images, an exclusion criterion removing objects lesser than or equal to 0.02 μm^2 was used to remove small background objects. Once the regions of interest in the image were properly outlined, data including number of puncta, intensity of puncta, area/ volume of puncta, among other measurements were exported and data analysed with GraphPad Prism. A minimum of 60 cells were analysed.

Supplementary Table 1: Summary of findings in dRTA kAE1 variant expressing cells compared to WT.

dRTA variant	*Transport Activity*	*Intracellular pH*	*LC3B Accumulation*	*Autophagy Flux*	*Cellular Lysosome size*	*Cellular lysosome number*	*Cellular mitochondrial abundance*	*Rescued Autophagy*
R295H	Unchanged	Unchanged	Unchanged	N/A	N/A	N/A	N/A	N/A
S525F	Reduced	Increased	Increased	Blocked downstream	Unchanged	Increased	Increased	Yes
R589H	Slightly Reduced	Increased	Increased	Blocked downstream	Increased	Unchanged	Increased	Yes

N/A, not applicable.

Supplementary Table 2: Summary of findings in intercalated cells from dRTA R607H knock-in (KI) relative to WT mice.

Genotype	*LC3B Accumulation*	*Intercalated Cell Lysosome size*	*Intercalated Cell lysosome number*	*Intercalated Cell mitochondrial abundance*
R607H KI/KI	Increased total LC3B	Increased	Increased	Increased

Supplementary Figures

Supplementary Figure 1: Two-hour incubation in pH 6.6 media with 0.033 μM nigericin reduces cytosolic pH to 6.9. (A) pHi of mIMCD3 cells incubated in either normal pH media of pH 6.6 media with 0.033 μM nigericin. Error bars correspond to mean ± SEM, n= minimum 4. ** P<0.01, using Student's t test. (B) Immunoblots of p53 with corresponding actin abundance in mIMCD3 cells at steady state and under chemically reduced intracellular pH conditions. (C) Graphical representation of ratio of p53 at steady state versus at low pHi in mIMCD3 kAE1 WT, S525F and R589H cells. Black circles indicate steady state cells and triangles indicate low pHi cells. Error bars correspond to mean ± SEM, n= 3. ** indicate P<0.01 using two-way ANOVA.

Supplementary Figure 2: dRTA kAE1 R607H knockin mice have lower abundance of intercalated cell marker B1 H^+-ATPase, lysosomal protease Cathepsin D and antioxidant protein PRDX 6 in intercalated cells-enriched primary cells. (A) Immunoblot of primary cells showing protein abundance of immature, intermediate and mature Cathepsin D (CTSD), antioxidant protein PRDX6 and intercalated cell marker B1 H^+-ATPase with corresponding GAPDH and actin abundance. The first two panels are from the same blot but the second one is cropped on the region around 48 kDa and lower, and exposed longer. Primary cells were obtained by magnetic sorting and lysed upon collection. (B-F) Graphical representation of protein abundance of immature CTSD, intermediate CTSD, mature CTSD, B1 H^+-ATPase and PRDX6 respectively in WT and knockin intercalated cell-enriched primary cells. Error bars correspond to mean ± SEM, n= minimum 4. * P<0.05, *** P<0.005 using Student's t test.

Supplementary Figure 3: Original immunoblots used for generating Figure 1.

Supplementary Figure 4: Original immunoblots used for generating Figure 2.

Supplementary Figure 5: Original immunoblots used for generating Figure 3.

References

1. Lashhab, R. *et al.* The kidney anion exchanger 1 affects tight junction properties via claudin-4. *Sci. Rep.* **9**, 3099 (2019).
2. Mungara, P. *et al.* Urinary Sodium Wasting and Disrupted Collecting Duct Function in Mice with dRTA-Causing SLC4A1 Mutations. *bioRxiv* 2024.08.21.608692 (2024). doi:10.1101/2024.08.21.608692
3. Saxena, V. *et al.* Kidney intercalated cells are phagocytic and acidify internalized uropathogenic Escherichia coli. *Nat. Commun.* **12**, (2021).
4. Sterling, D. & Casey, J. R. Transport activity of AE3 chloride/bicarbonate anion-exchange proteins and their regulation by intracellular pH. *Biochem J* **344 Pt 1**, 221–229 (1999).
5. Stirling, D. R. *et al.* CellProfiler 4: improvements in speed, utility and usability. *BMC Bioinformatics* **22**, (2021).
6. Schindelin, J. *et al.* Fiji: An open-source platform for biological-image analysis. *Nature*

Methods **9**, 676–682 (2012).

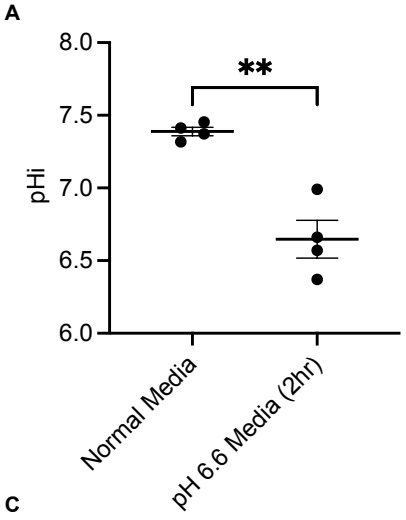

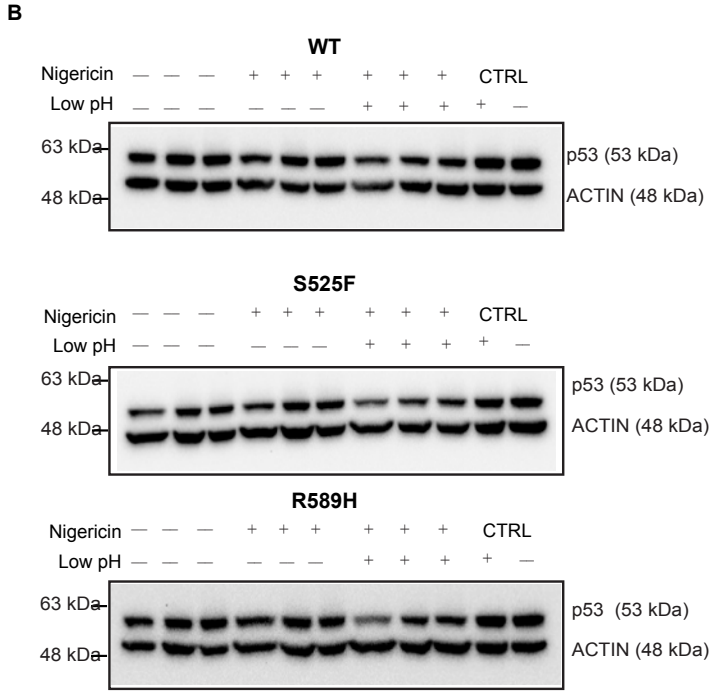

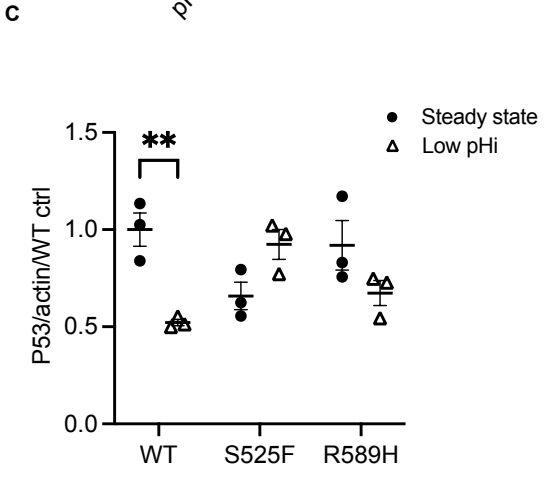

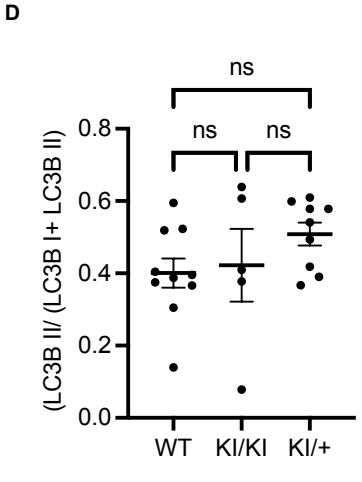

Supplementary Figure 1 Essuman et al.

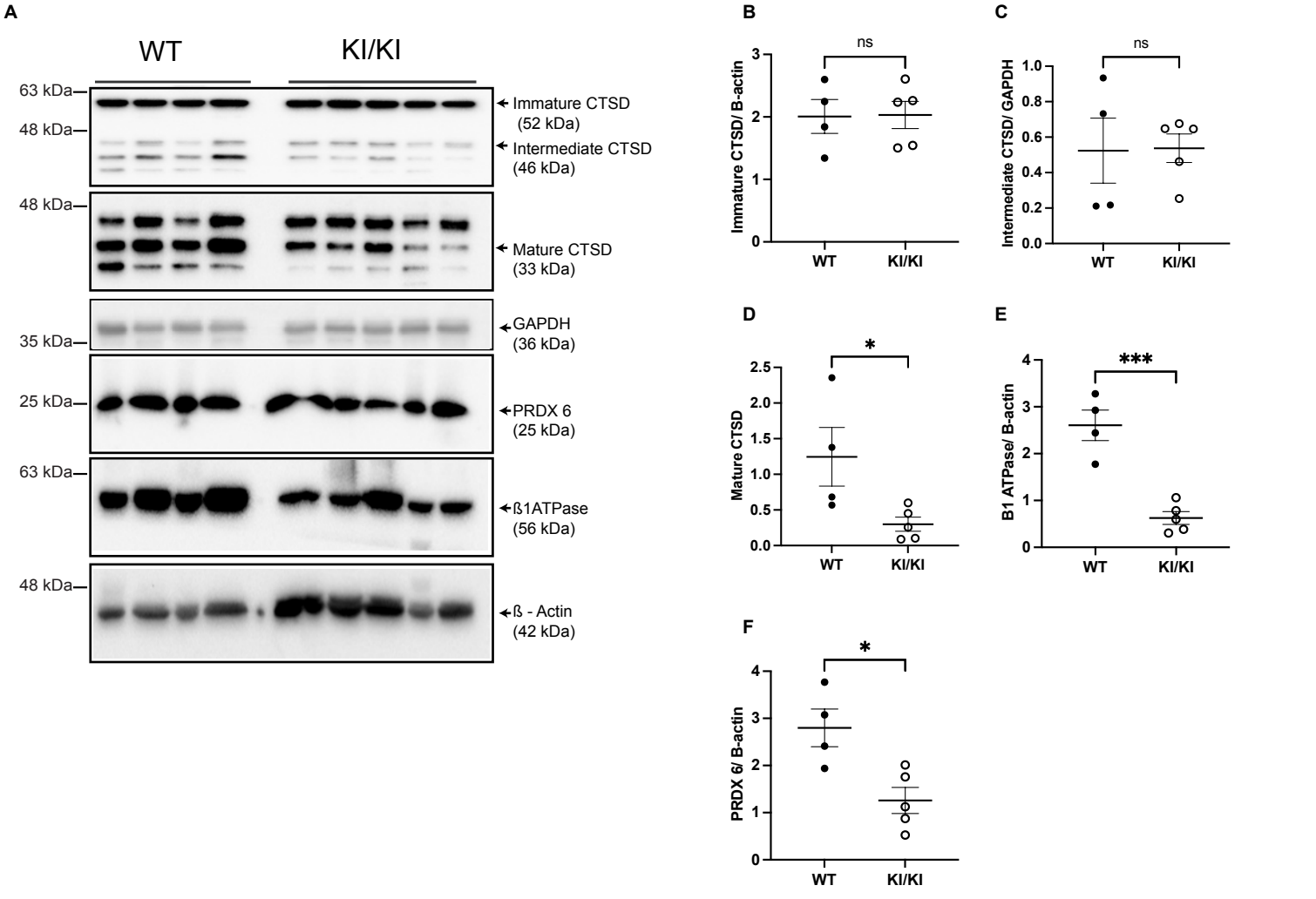

Supplementary Figure 2 Essuman et al.

Panel B

kAE1

Actin

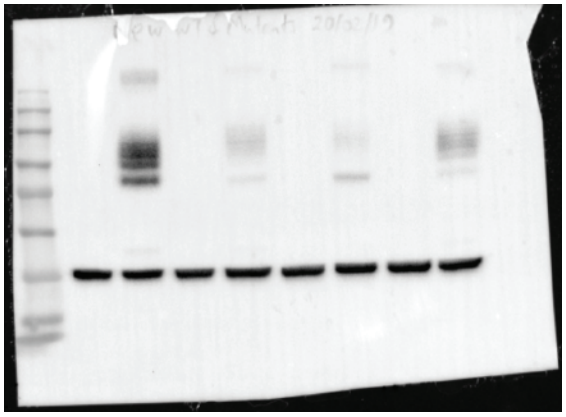

Panel D

kAE1

Actin

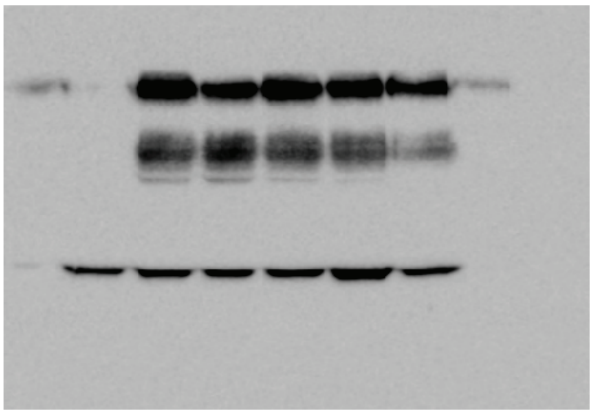

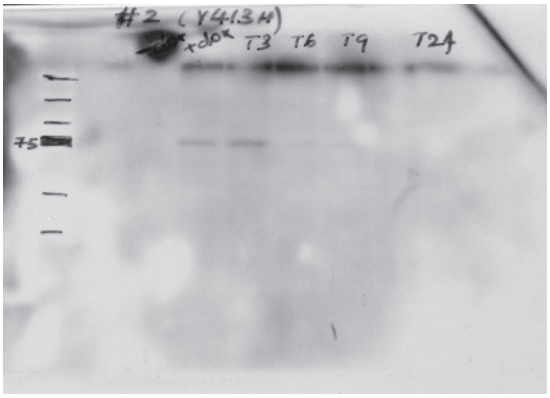

kAE1

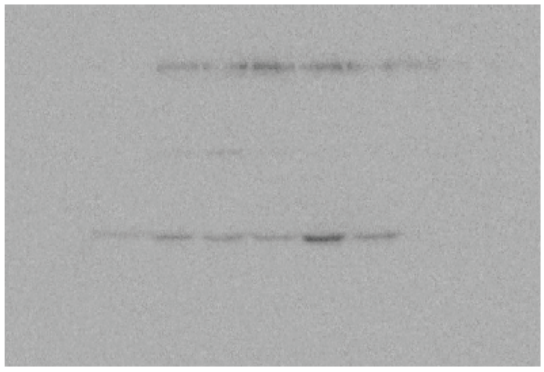

Actin

Supplementary figure 3 Essuman et al.

Panel A

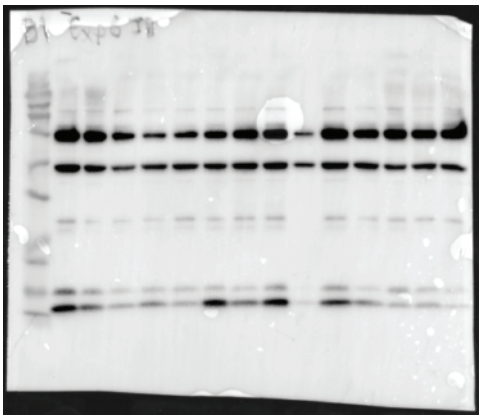

Panel B

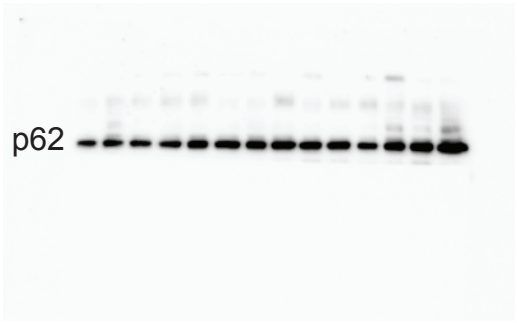

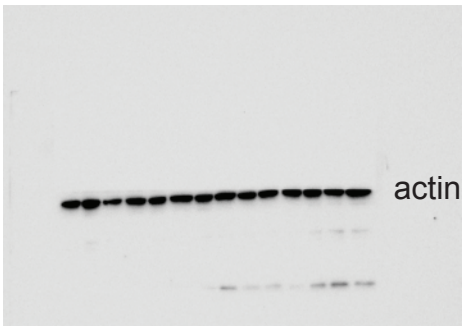

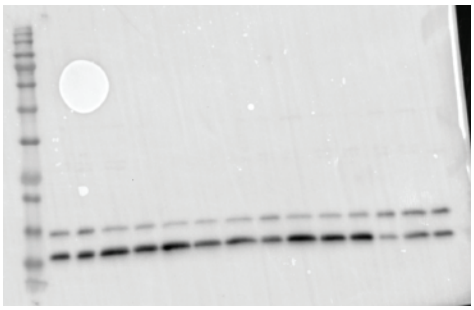

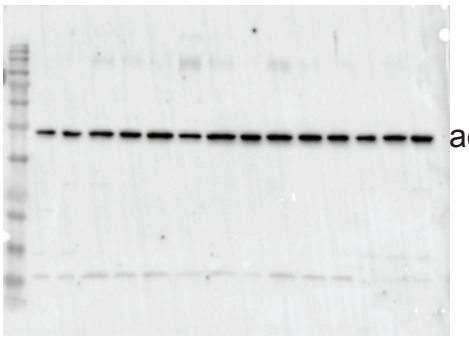

Panel C

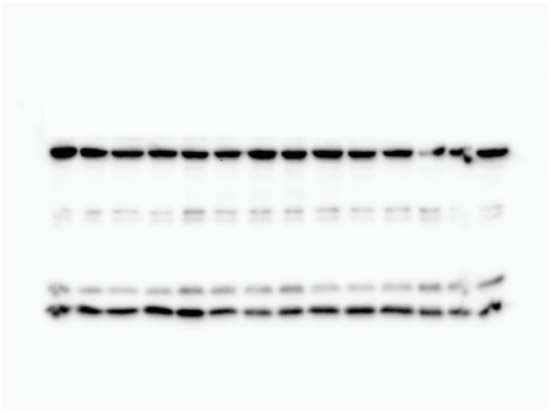

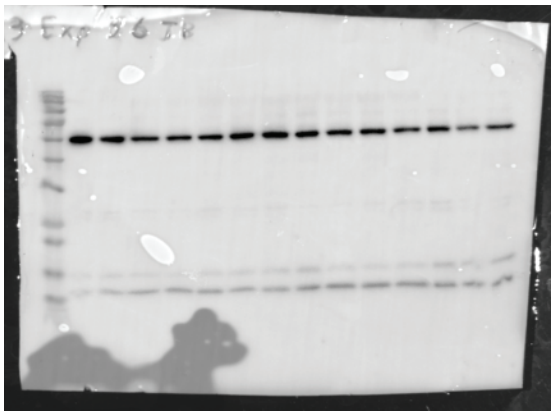

Panel J

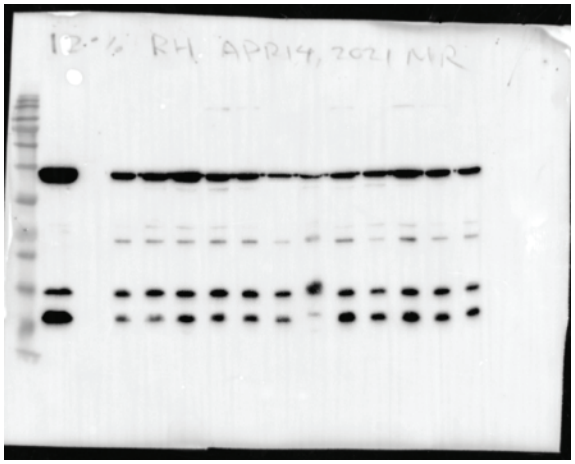

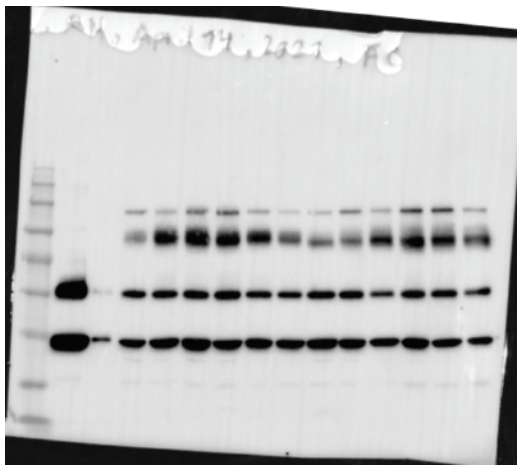

Supplementary figure 4 Essuman et al.

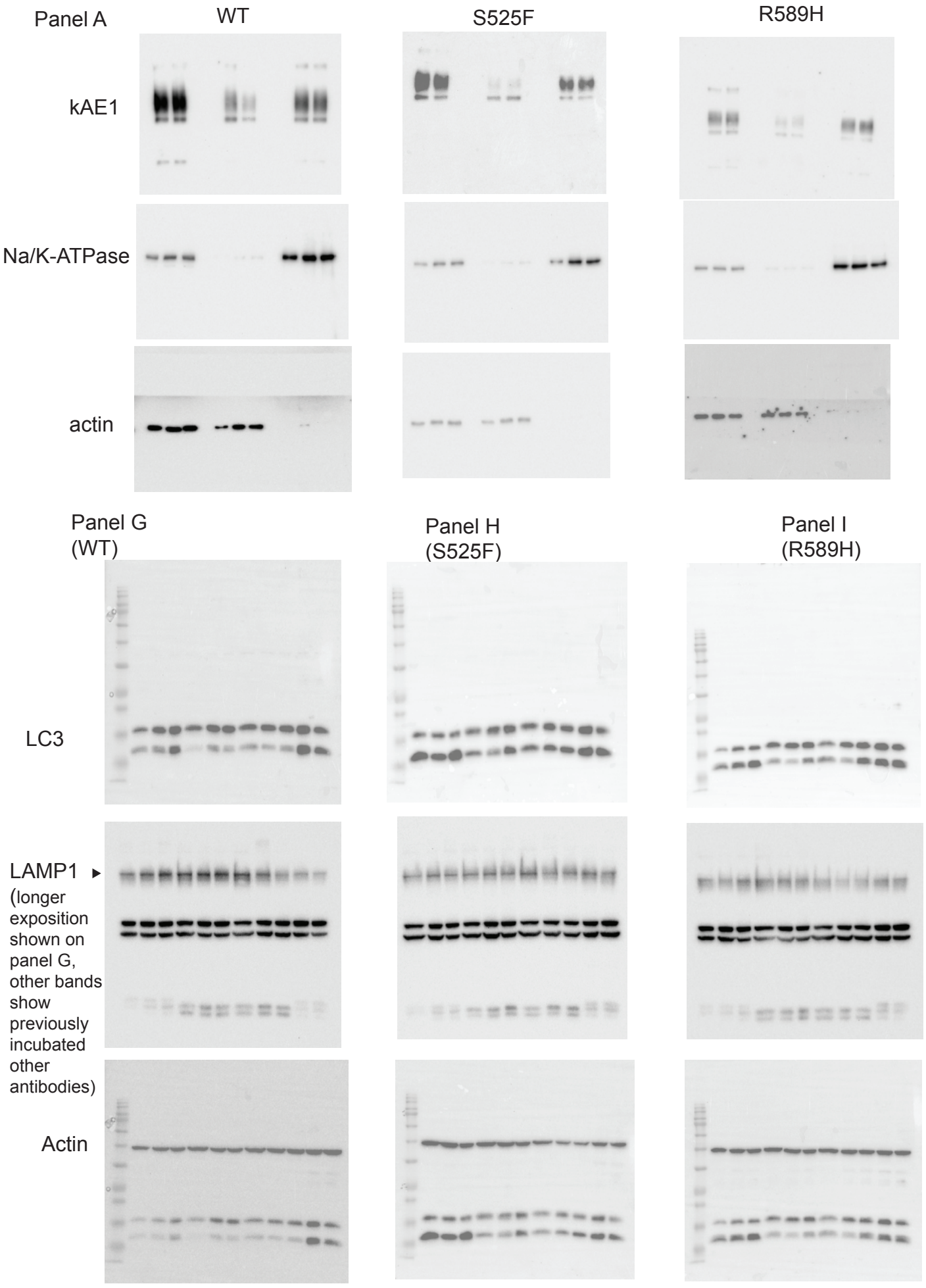

Supplementary figure 5 Essuman et al.